ISSN 0016-8521, Geotectonics, 2022, Vol. 56, No. 4, pp. 405–434. © Pleiades Publishing, Inc., 2022.
Russian Text © The Author(s), 2022, published in Geotektonika, 2022, No. 4, pp. 3–34.

Late Precambrian Rhyolite–Granite Volcanic–Plutonic Associations of the Southern Ulutau (Central Kazakhstan)

A. A. Tretyakov[a], *, K. E. Degtyarev[a], N. A. Kanygina[a], V. P. Kovach[b], and B. V. Fedorov[c]

[a] *Geological Institute, Russian Academy of Sciences, Moscow, 119017 Russia*

[b] *Institute of Precambrian Geology and Geochronology, Russian Academy of Sciences, St. Petersburg, 199034 Russia*

[c] *Sergo Ordzhonikidze Russian State University for Geological Prospecting, 23 ul. Miklukho-Maklaya, Moscow, 117997 Russia*

**e-mail: and8486@yandex.ru*

Received May 24, 2022; revised June 6, 2022; accepted June 25, 2022

Abstract—The results of a study of Late Precambrian effusive and plutonic rocks of the Dyusembai and Aktass volcanic–plutonic associations of the western part of the Southern Ulutau are reported. A U–Th–Pb isotope–geochronological study of accessory zircons (SHRIMP II) showed that the formation of rhyolite–granite associations occurred in the second half of the Tonian in the Neoproterozoic (~830 Ma, Dyusembai association, and ~800–790 Ma, Aktass association). The formation of parental melts for effusive and plutonic rocks of both associations occurred via dehydration melting of metatonalite (metagreywacke) formations of the Early Precambrian continental crust in an intraplate environment. The Neoproterozoic evolution of the Southern Ulutau took place in an environment of an active continental margin. The formations of the eastern part of the Southern Ulutau were formed within the ensialic island arc, while the western part, in the area of riftogenic magmatism, upon extension in the rear area. The Tonian magmatism in the Southern Ulutau, as well as in the other terranes of the Ulutau–Moyunkum Group, indicates their incorporation into the basement of a large volcanic–plutonic belt marking subduction of the oceanic lithosphere beneath the northwestern margin of the Rodinia supercontinent.

Keywords: Neoproterozoic, rhyolite, granites, U–Pb dating, rifting, subduction, Tarim, Rodinia

DOI: 10.1134/S0016852122040082

INTRODUCTION

Intra- and marginal-continental types can be distinguished in volcanic–plutonic belts, which are among the largest structures of the Earth. The origin of marginal-continental belts is associated with the evolution of suprasubduction igneous systems confined to the zones of convergence of the oceanic and continental plates (belts of the Andean active continental margin). The formation of intracontinental belts may be controlled by convergent boundaries accompanied by collision (Alpine–Himalayan Belt), or due to the development of rifting processes accompanied by lithosphere extension and rise of the mantle diapir (belts of the East African rift system).

The structures of different types of volcanic–plutonic belts involve felsic igneous rocks, often forming volcanic–plutonic rhyolite–granite associations. They combine volcanic and intrusive formations with similar patterns of the chemical and isotope compositions and similar age estimates, which indicate their relationship with the evolution of a single parental melt.

Rhyolite-granite associations of intracontinental belts are usually the end-members of contrasting series in which they are associated with igneous rocks of ultramafic and mafic compositions with a high alkalinity. In this case, felsic rocks are considered as the result of the mantle–crust interaction caused by underplating of mafic melts and the formation of intracrustal melt chambers [18, 57].

Felsic volcanic rocks and granitoids of marginal-continental belts are often associated with rocks of the mafic and intermediate compositions of with calc-alkaline specialization forming differentiated series [8, 45]. The origin of felsic varieties in this case is considered as the final result of the evolution of melts, including their generation in the suprasubduction setting of the active margin, followed by the processes of crystallization differentiation and assimilation [8, 45]. At the same time, rifting processes in the rear and axial zones of the continental-marginal belts may lead to the formation of contrasting series as well [15].

The Precambrian volcanic–plutonic belts are of particular interest, since their complexes provide information on the evolution of the convergence and rifting

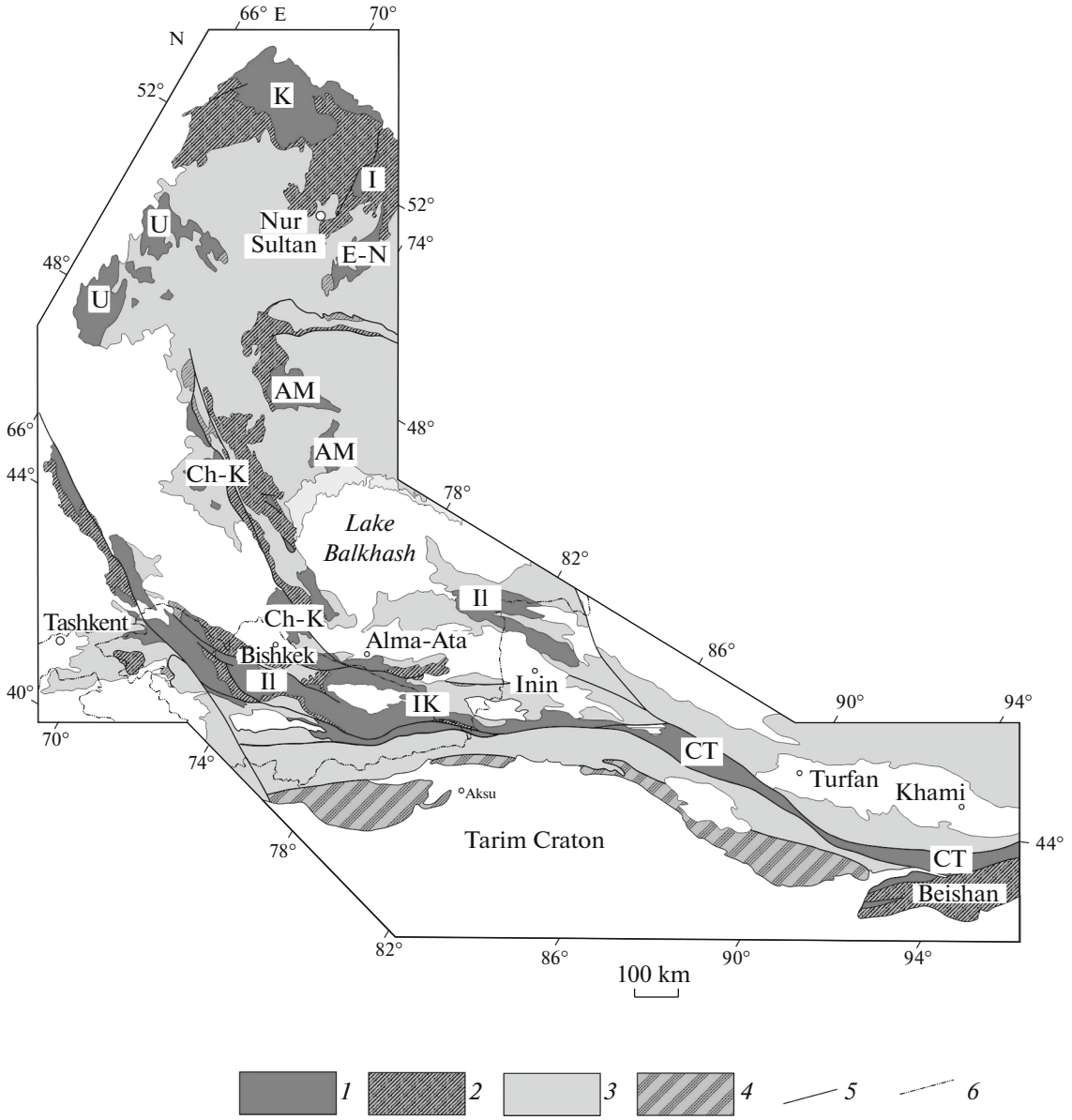

Fig. 1. The scheme of the location of Precambrian terranes in the western part of the Central Asian Foldbelt. Precambrian terranes: K, Kokchetav; I, Ishkeolmes; E-N, Erementau–Niyaz; AM, Aktau–Mointy; U, Ulutau; Ch-K, Chuya–Kendyktas; Il, Ili; IK, Issyk-Kul; CT, Central Tien Shan. (*1*) Precambrian terranes; (*2–4*) complexes: (*2*) Lower Paleozoic volcanic–sedimentary, (*3*) Middle–Upper Paleozoic volcanic–sedimentary, (*4*) Precambrian and Paleozoic complexes of the Tarim Craton; (*5*) large faults; (*6*) State border.

zones, which controlled the paleotectonic development and growth of the continental crust of the Precambrian supercontinents (Rodinia, Nuna) [46, 47, 54].

The opening of the oceans, breakup of supercontinents, and repeated collisional events in the Phanerozoic resulted in fragmentation of large Precambrian structures, including volcanic–plutonic belts, and their complexes experienced significant displacements, deformations, and metamorphism.

In the western part of the Central Asian Belt, covering the territories of Kazakhstan, Kyrgyzstan, and NW China, Precambrian formations are involved in the structures of terranes of various sizes located among the Lower Paleozoic accretionary and island-arc complexes (Fig. 1). As a result of the study of the Meso- and Neoproterozoic complexes, the terranes of this part of the belt were divided into two groups that had different tectonic–magmatic evolutions in the Late Precambrian: the northeastern, Issedon (Kokchetav, Ishkeolmes, Aktau–Dzhungar, Issyk-Kul, and Ili terranes), and southwestern, Ulutau-Moyunkum (Ulutau, Karatau–Dzhebagli, Middle Tien Shan, Chuya–Kendyktas, and Zheltav terranes) terranes [23]. Recent studies have shown that the fragments of the Precambrian volcanic–plutonic belts are parts of the

structure of the Precambrian terranes of both groups. For example, sheared rhyolite, trachyrhyolite, and granitoids, the formation of which was associated with the evolution of two volcanic–plutonic belts with ages of ~1150 and ~900 Ma, are widespread within the terranes of the Issedon Group [23, 34, 66]. The isotope–geochemical patterns of these volcanic rocks and granite make them similar to A-type granite and indicate the formation of melts in the intraplate settings upon melting of the Early Precambrian continental crust [1, 23].

The younger igneous complexes are involved in the structure of terranes of the Ulutau–Moyunkum Group [23]. These are metamorphosed felsic volcanic rocks and granitoids, including those altered under the high-pressure conditions.

The geochronological data obtained in recent years indicate the formation of these rocks within the Neoproterozoic (830–770 Ma) volcanic–plutonic belt [23, 37, 60, 63]. However, as the geochronological data are insufficient and volcanogenic sequences are poorly preserved and metamorphosed significantly, it is difficult to correlate the volcanic and plutonic complexes of different terranes. The crustal Nd isotope–geochemical characteristics of felsic rocks, the lack of their spatial and genetic relationship with rocks of more basic composition often do not allow us to estimate the conditions for the formation of melts, which makes difficult to reconstruct the geodynamic settings for the formation of complexes of the Neoproterozoic volcanic–plutonic belt. Therefore, the most interesting object for research is the Ulutau Terrane, located in the west of Central Kazakhstan; it includes Neoproterozoic granitoids and felsic volcanic rocks, characterized by completeness of sections and low degree of metamorphism.

THE STRUCTURAL PATTERNS OF PRE-EDIACARAN COMPLEXES OF THE SOUTHERN ULUTAU

The pre-Ediacaran complexes of the Ulutau Terrane are poorly metamorphosed volcanogenic, volcanogenic–sedimentary, and granitoid complexes, which are most widespread in its southern part (Southern Ulutau). The differentiated (basalt–andesite–rhyolite) volcanogenic–sedimentary rocks, associated with chemogenic ferruginous quartzite, shale, and limestone (Aralbai, Karsakpai and Beleuta groups) occur in the eastern part of the Southern Ulutau (Karsakpai Zone); an amphibolite-gneiss complex (Balazhezda Formation) is located structurally below (Figs. 2, 3) [13, 14].

The geochronological studies carried out in recent years provided U–Pb age estimates of accessory zircon grains from felsic volcanic rocks of the Aralbay, Beleuta, Karsakpai groups, as well as from metamagmatic rocks of the Balazhezda Group, these data provide evidence for the Late Neoproterozoic (~740–760 Ma) age of these rocks [10–12].

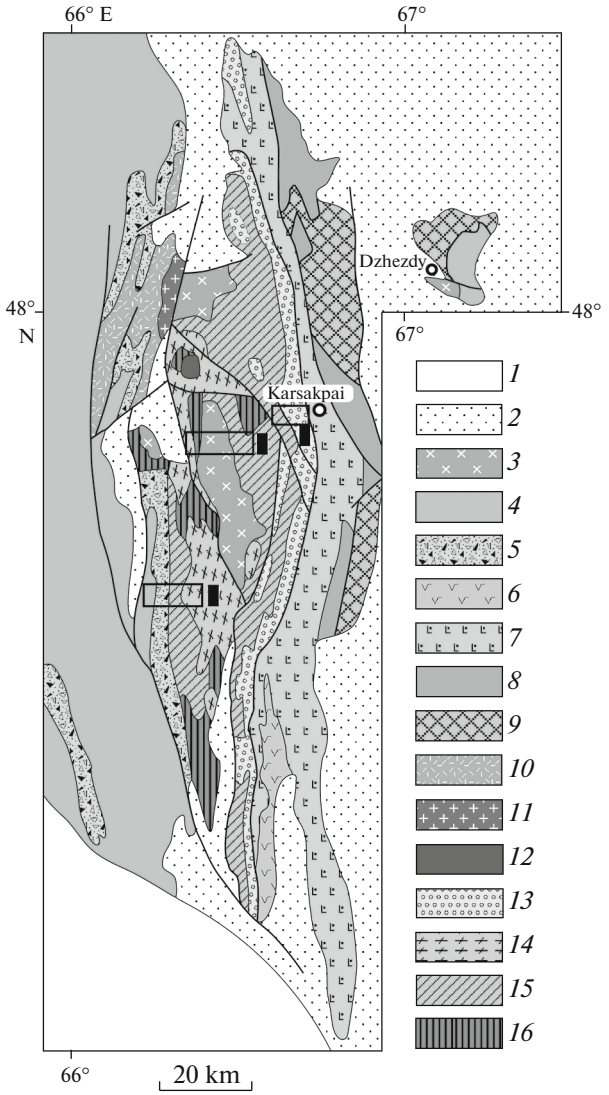

Fig. 2. A scheme of the geological structure of the Southern Ulutau, modified after [13]. Areas of detailed studies (outline) are shown: (1) area of the Dyusembai River, (2) area of the Koktal and Akyrlysai rivers, (3) area of the Bereke River. (*1*) Mesozoic–Cenozoic deposits; (*2*) Devonian and Carboniferous volcanogenic sequences; (*3*) Paleozoic granitoids; (*4*) Lower Paleozoic siliceous–terrigenous and terrigenous sequences; (*5*) Ediacaran volcanogenic–sedimentary and coarse clastic sequences; (*6–9*) Neoproterozoic metamorphosed volcanic–sedimentary sequences of the eastern part of the Southern Ulutau: (*6*) Beleuta Group, (*7*) Karsakpai Group, (*8*) Aralbai Group, (*9*) Balazhezdin Group; (*10–15*) Neoproterozoic metamorphosed volcanic–sedimentary sequences and plutonic complexes of the western part of the Southern Ulutau (Maityubinsk Zone): (*10*) Koksu Group, (*11*) Aktass granite complex, (*12*) Karsakpai Complex of alkaline syenite, (*13*) Bozdak Group, (*14*) Zhaunkar granite complex, (*15*) Maityubinsk Group, (*16*) Mesoproterozoic volcanic sequences of the Zhiidinskaya Group.

The distinctive feature of the western part of the Southern Ulutau (Maityubinsk Zone) is the wide abundance of poorly metamorphosed felsic volcanic and volcanic–sedimentary rocks (Maityuinsk and

Koksui groups), which are associated with large granitoid massifs (Zhaunkar and Aktass complexes) (see Figs. 2, 3). The Maityubinsk Group is underlain by the Zhiida Group, composed of metamorphosed felsic and basic volcanic rocks, sheared terrigenous and volcanic–sedimentary rocks. The sequences of felsic volcanic rocks that are part of the Maityubinsk Group are overlain by black shale, quartzite–shale, and coarse clastic volcanic–sedimentary sequences (Kumola, Ushtoba, Bozdak, and other formations) [2, 13]. The U–Pb age estimates were previously obtained for granite of the Zhaunkar and Aktass complexes and felsic volcanic rocks of the Koksu Group, indicating the Neoproterozoic (~800–830 Ma) age of their formation [5, 23].

In our research we report the results of the geological, geochronological, and isotope–geochemical studies of the Neoproterozoic rhyolite–granite complexes of the Maityubinsk Zone in the western part of the Southern Ulutau.

THE STRUCTURE AND MINERAL COMPOSITION OF NEOPROTEROZOIC VOLCANIC AND PLUTONIC COMPLEXES

Two associations of felsic volcanic and plutonic rocks similar in age, namely Dyusembai and Aktass, may be distinguished in the western part of the Southern Ulutau.

Dyusembai Association

The complexes of the Dyusembai association compose most of the Maityubinsk Zone, where they include felsic volcanic rocks of the Dyusembai, Zhaunkar, and, probably, Tatpen formations of the Maityubinsk Group, as well as granitoids of the Zhaunkar Complex (Figs. 2, 3).

Rocks of the Dyusembai Formation. Volcanogenic rocks of the Dyusembai Formation were studied in the stratotype section in the upper reaches of the Dyusembai River (central part of the Maityubinsk Zone). Sheared felsic volcanic rocks with a fluidal structure and tuff of the same composition of the Dyusembai Formation (up to 2000-m thick) form the core of a large meridional antiform there (Fig. 4).

These rocks with unclear relationships are underlain by sericite–chlorite–quartz schist and quartz schist, which are conventionally related to the upper section of the Zhiida Group. The rocks of the Dyusembai Formation are unconformably overlain by a thin member of carbonaceous quartzite and quartz schists on the southern periclinal and eastern flank of the antiform; most likely, with a tectonic contact, Dyusembai Formation is overlain by sheared felsic volcanic rocks related to the Zhaunkar Formation.

Felsic volcanic rocks are unconformably overlain by volcanogenic–sedimentary sequence of variegated composition (conglomerate, sericite–feldspar, quartz–biotite–sericite schist, mafic and felsic volcanic rocks, marble, ferruginous and graphite quartzite) on the flanks of the antiform and its southern periclinal closure; these rocks are identified as the Koldybaishokinsk and Zhilandysai formations [13].

Rocks of the Zhaunkar Formation. These effusive rocks were studied in the west of the Maityubinsk Zone in the area of the Koktal and Akyrlysai rivers, where the Neoproterozoic complexes are involved in the structure of the eastern flank of the large synform (Fig. 5).

The lowest position in the structure is occupied by coarse-grained sheared granite of the Zhaunkar Massif of the same complex. Granite is unconformably overlain by a thin (up to 60 m) member of blastopsammitic quartzite and carbonaceous shale, which is a marker and extends for a long distance [13].

The rocks of the Zhaunkar Formation represented by sheared fluidal felsic effusive rocks and tuff, often with lenticular fiamme, with a total thickness of up to 1500 m, occur structurally higher, probably with tectonic contact. Their contacts with effusive rocks of the Zhaunkar Formation are most likely tectonic as well (Fig. 5).

Felsic effusive rocks, which dominate in both formations, experienced metamorphism, expressed in schistosity and in some places a banded structure. The groundmass in the rocks is recrystallized and transformed into a fine-grained lepidogranoblastic aggregate consisting of quartz, alkali feldspar, acid plagioclase, biotite, muscovite, chlorite, zoisite, and ore mineral.

The predominant phenocrysts are orthoclase and plagioclase (oligoclase–andesite and oligoclase–albite), and quartz, while biotite and ilmenite are the minor ones. Among the accessory minerals are apatite and zircon.

Orthoclase and quartz are phenocrysts in rocks of normal alkalinity; plagioclase (oligoclase–albite) and biotite are the minor phases. Among the accessory minerals are apatite and zircon.

Zhaunkar Granite Complex unites several intrusions (North Sarysai, Kulanbai, Zhaunkar, and Zhiida) in the axial part of the Maityubinsk Zone, intruding volcanogenic–sedimentary rocks of the Zhiida Group, as well as felsic volcanic rocks of the Dyusembay Formation. The structure of the intrusions is dominated by sheared coarse-grained, porphyritic leucocratic granite of the major intrusive phase. Less common is medium-grained leucogranite of the late intrusive phase.

Aktass Association

The complexes of the Aktass association mainly occur in the west of the Southern Ulutau, where they include volcanic rocks of the Koksui Group and granite of the Aktass Formation. This association includes

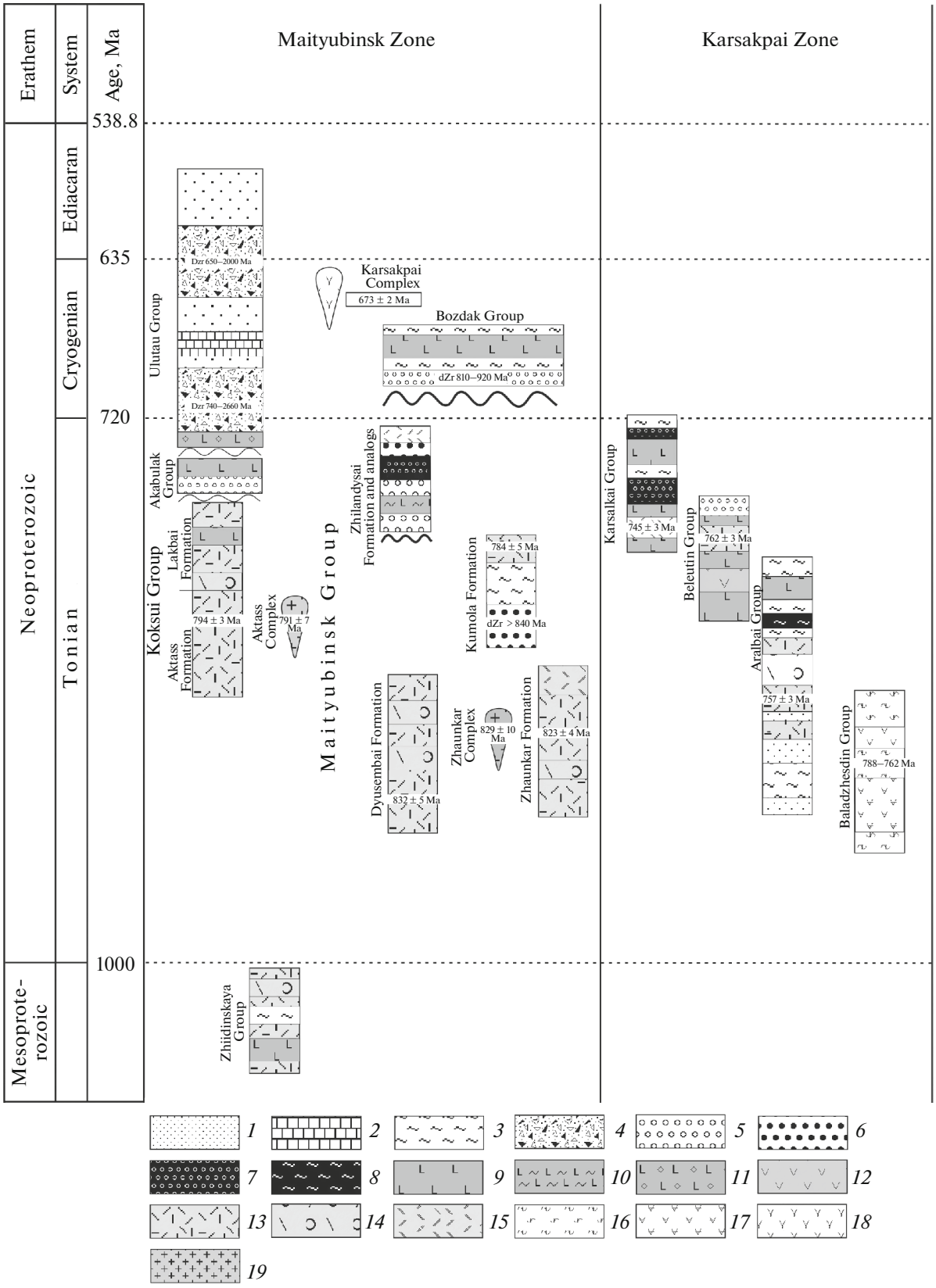

Fig. 3. The correlation scheme of Precambrian stratified and plutonic complexes of various zones of the Southern Ulutau. (*1*) Sandstone; (*2*) limestone; (*3*) quartz–feldspar schist, phyllite; (*4*) tillite-like conglomerate; (*5*) conglomerate; (*6*) quartzite, quartz sandstone; (*7*) ferruginous quartzite; (*8*) ferruginous shale; (*9*) basalt; (*10*) tuff siltstone and tuffite of the basic composition; (*11*) basic tuff conglomerate; (*12*) andesite; (*13*) rhyolite; (*14*) felsic tuff conglomerate; (*15*) felsic tuff; (*16*) shale and gneiss; (*17*) amphibolite and amphibole schist; (*18*) syenite; (*19*) granitoids.

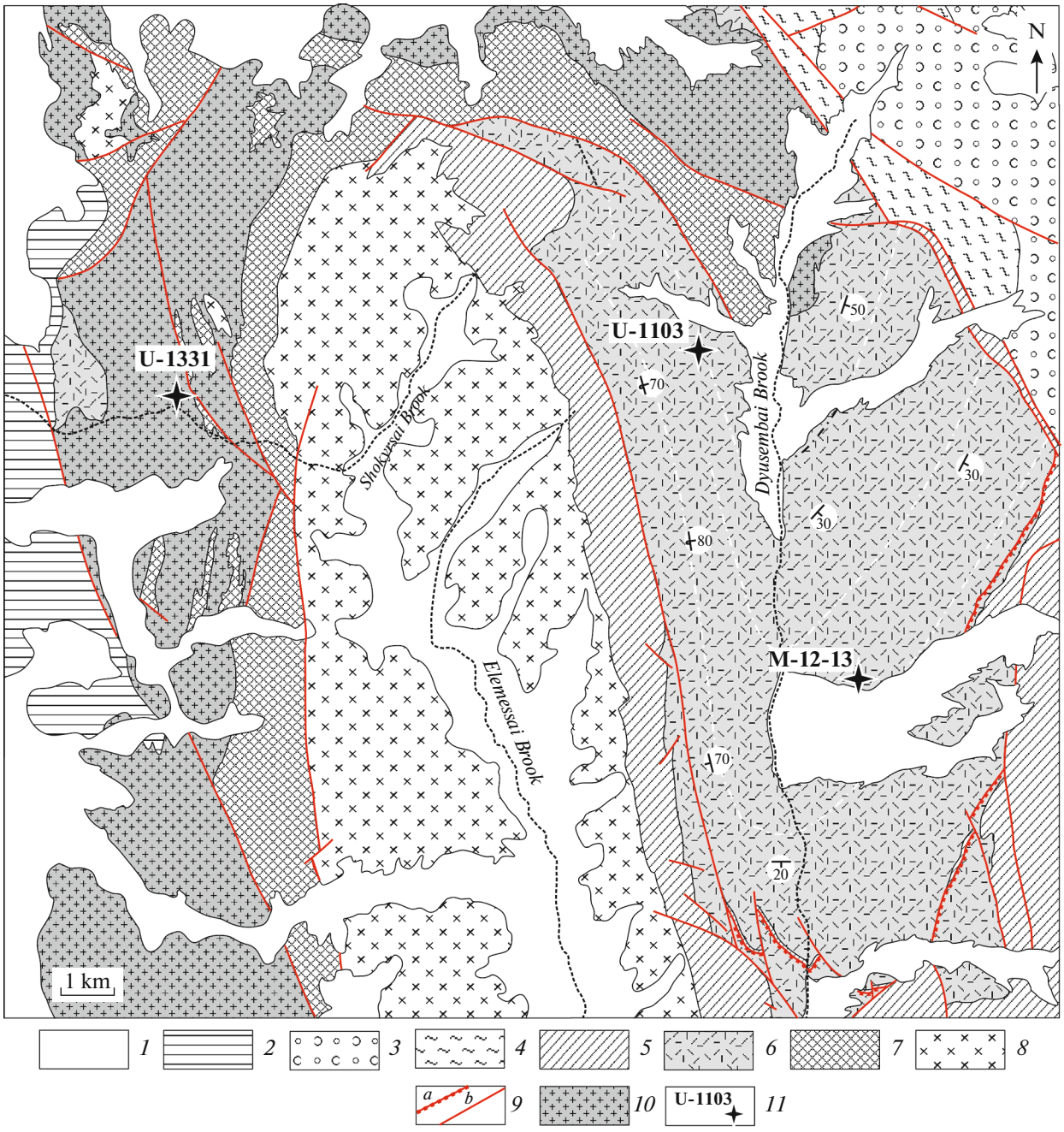

Fig. 4. The geological scheme of the site of detailed study in the area of the Dusembai River. (*1*) Cenozoic deposits; (*2*) Devonian and Carboniferous volcanogenic and sedimentary rocks; (*3*) conglomerate, feldspar shale, tuff, tuff conglomerate, effusive rocks of the basic composition of the Bozdak Group; (*4*) quartzite, quartz sandstone, phyllite-like shale of the Kumola Formation; (*5*) conglomerate, sericite–feldspar, quartz–biotite–sericite schist, marble, ferruginous and graphitic quartzite, tuff and effusive rocks of the basic and felsic compositions of the Koldybaishokinskaya and Zhilandysai formations; (*6*) felsic effusive rocks and tuff of the Dyusembai Formation; (*7*) quartzite and phyllite-like schist of the Zhiidinskaya Group; (*8*) Paleozoic granitoids; (*9*) faults: (*a*) thrusts, (*b*) others; (*10*) granitoids of the Zhaunkar Complex (North Sarysai Massif); (*11*) sampling sites and nos. of geochronological samples.

felsic effusive rocks of the upper part of the Kumola Formation related to the Maityubinsk Group in the east of the Maityubinsk Zone.

The rocks of the Koksui Group and granitoids of the Aktass Formation were studied in the northwestern marginal part of the Maityubinsk Zone near the boundary with the Ediacaran–Lower Paleozoic formations of the Baikonur Zone (Fig. 2).

Rocks of the Koksui Group. This group is composed of sheared felsic volcanic rocks and tuff in the lower

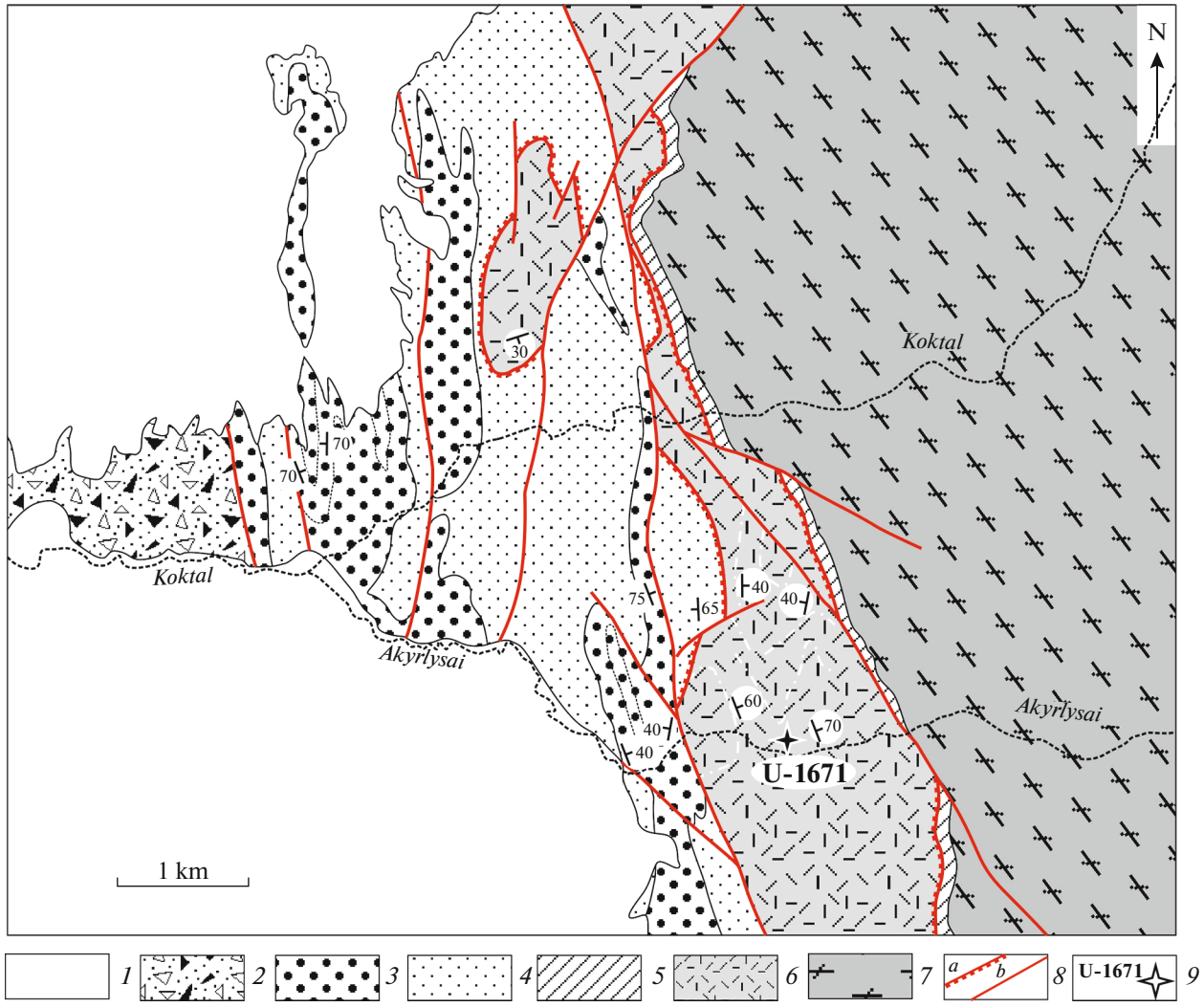

Fig. 5. The geological scheme of the site of detailed study in the area of the Koktal and Akyrlysai rivers. (*1*) Cenozoic deposits; (*2*) tillite-like conglomerate, phyllite-like schist of the Satan Formation; (*3–4*) Ushtoba Formation: (*3*) quartzite, quartz schist, (*4*) sericite–quartz schist; (*5–6*) Zhaunkar Formation: (*5*) quartzite and carbonaceous shale, (*6*) felsic volcanic rocks and tuff; (*7*) granitoids of the Zhaunkar Complex; (*8*) faults: (*a*) thrusts, (*b*) others; (*9*) sampling sites and nos. of geochronological samples.

part and effusive rocks, tuff, and rhyolitic ignimbrite with horizons of sandstone and conglomerate (the Lakbai Formation) in the upper part. The total thickness of the Koksui Group reaches 1500 m.

The effusive rocks of the Koksui Group are represented by sheared rhyolite with massive, less often fluidal structure. Quartz and orthoclase phenocrysts occur in a fine-grained lepidogranoblastic groundmass consisting of quartz, alkali feldspar, acid plagioclase, biotite, and muscovite.

Granite of the Aktass Formation. This rock composes linearly elongated bodies (Aktass and Ugyrlytau intrusions) with a length up to 20 km and width of 3 km or less, which are mainly formed by coarse-grained, sometimes porphyritic, biotite granite.

Rocks of the Kumola Formation. This formation is mainly distributed in the east of the Maityubinsk Zone. The lower part of the formation is composed of alternating quartzite, quartz schist, with a subordinate amount of phyllite; there is a unit of fluidal felsic volcanic rocks and tuff with a thickness up to 300 m at the top of the section. The rocks of the upper part of the Kumola Formation were studied on the left bank of the Bereke River, where they form the western flank of a large syncline, overlain by boulder conglomerate and basic effusive rocks of the Bozdak Group without visible unconformity (Fig. 6).

METHODS

The analysis for the major rock-forming elements by X-ray fluorescence method using an S4 PIONEER sequential wave-dispersive spectrometer manufactured by Bruker AXS (Germany) with an X-ray tube with a power of 4 kW, Rh anode, and a 75 μm thick Be

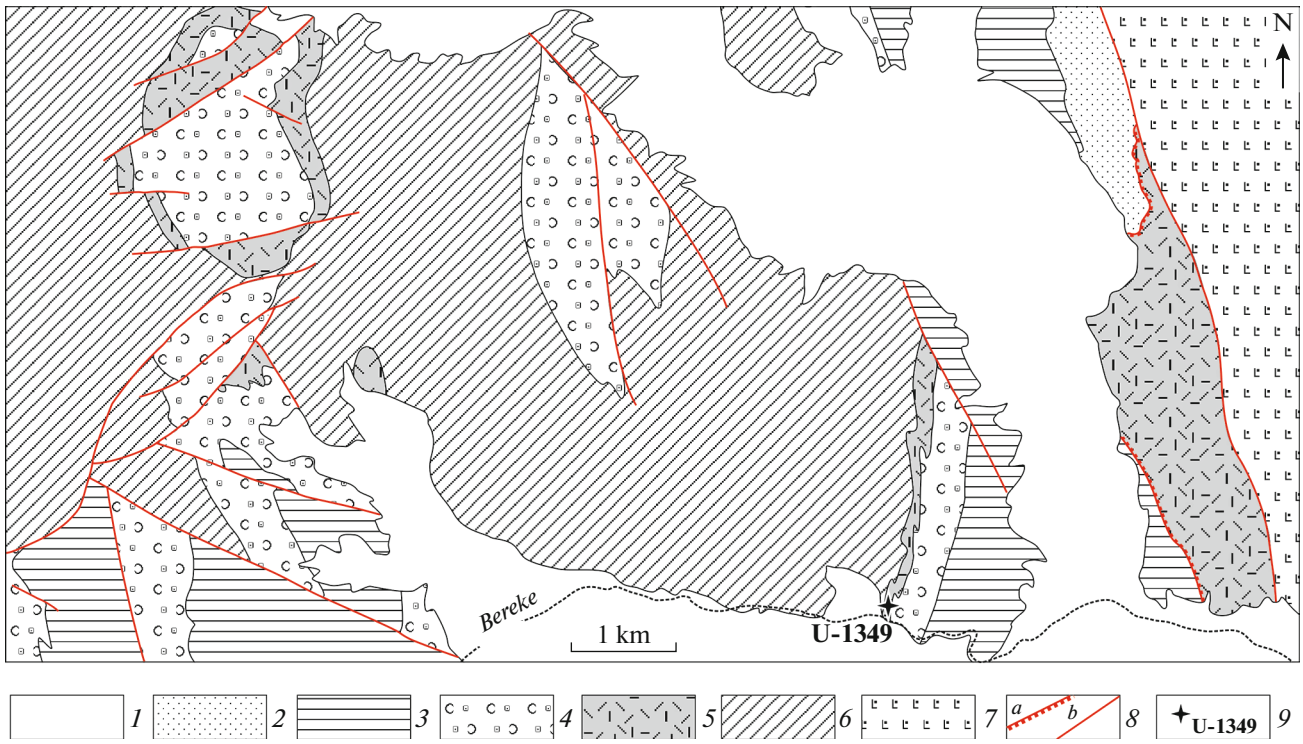

Fig. 6. The geological scheme of the site in the area of the Bereke River. (*1*) Cenozoic deposits; (*2–4*) Bozdak Group: (*2*) quartzite, quartz schist, quartz–feldspar schist, phyllite-like schist, (*3*) quartz–sericite–chlorite schist, conglomerate, mafic and felsic effusive rocks, (*4*) mafic tuff and effusive rocks; (*5–6*) Kumola Formation: (*5*) felsic effusive rocks, (*6*) quartzite and quartz schist; (*7*) effusive rocks and tuff of the basic composition of the Karsakpai Group; (*8*) faults: (*a*) thrusts, (*b*) others; (*9*) sampling sites with nos. of geochronological samples.

window was carried out at the Laboratory of Chemical–Analytical Studies, Geological Institute, Russian Academy of Sciences (Moscow, Russia). The contents of trace components in the rocks were determined by the ICP MS method at the Analytical Certification and Testing Center of the Institute of Microelectronics and Highly Pure Materials, Russian Academy of Sciences (Moscow, Russia).

The Sm–Nd isotope data were obtained at the Institute of Precambrian Geology and Geochronology, Russian Academy of Sciences (St. Petersburg, Russia). Approximately 100 mg of powdered samples, to which a mixed ^{149}Sm–^{150}Nd tracer was added, were decomposed in Teflon bottles in a mixture of HF, HNO_3, and $HClO_4$. REEs were extracted by the standard cation exchange chromatography on BioRad AG1-X8 resin columns (200–400 mesh), while Sm and Nd were extracted by chromatography on LN-Spec (100–150 mesh) columns.

The Sm and Nd isotope compositions were analyzed on a TRITON TI multicollector mass spectrometer in static mode. The measured $^{143}Nd/^{144}Nd$ ratios were normalized to $^{146}Nd/^{144}Nd = 0.7219$ and reduced to $^{143}Nd/^{144}Nd = 0.512115$ in the JNdi-1 Nd standard. The blank run level was 0.05–0.2 ng Sm and 0.1–0.5 ng Nd.

The accuracy of the analysis of Sm and Nd concentrations was ±0.5%; that of the $^{147}Sm/^{144}Nd$ isotope ratios was ±0.5%; and for the $^{143}Nd/^{144}Nd$ isotope ratios it was ±0.005% (2σ). The values of εNd(t) and model ages TNd(DM), modern values of the homogeneous chondrite reservoir (CHUR), after [35] ($^{143}Nd/^{144}Nd = 0.512638$, $^{147}Sm/^{144}Nd = 0.1967$), and DM, after [32] ($^{143}Nd/^{144}Nd = 0.513151$, $^{147}Sm/^{144}Nd = 0.21365$) were used for calculations.

The U–Pb geochronological studies of accessory zircons were carried out to substantiate the age of plutonic and volcanic rocks. The extraction of zircon from rhyolite was carried out by the standard methodology using heavy liquids. Zircon grains were mounted in epoxy along with standard TEMORA and 91500 zircon grains, and then ground to about half of their thickness and polished. Photomicrographs taken on a Camscan MX 2500S scanning electron microscope in secondary electron and cathode luminescence modes were used to select areas of zircon grains for local geochronological studies.

The U–Pb (SIMS) geochronological studies of zircons were carried out on a SHRIMP-II secondary ion microprobe at the Center for Isotope Studies of the Russian Geological Research Institute (St. Petersburg, Russia). The U and Pb isotope ratios were mea-

Table 1. The characteristics of the samples used for the isotope–geochronological U–Pb studies and the obtained age estimates

Sample	N	E	Location	Rock	Formation/Complex	Age (Ma)
Dyusembai volcanic–plutonic association						
U-1103	47°46′34.80″	66°31′52.10″	Dyusembai River	Rhyolite	Dyusembai	836 ± 6
U-1671	47°22′57.10″	66°22′56.70″	Akyrlysai River	Trachydacite	Zhaunkar	823 ± 5
U-1331	47°46′46.3″	66°24′47.2″	Shokyrsai River	Leucogranite	Zhaunkar	**829 ± 10**
Aktass volcanic–plutonic association						
U-1349	47°50′31.29″	66°40′38.63″	Bereke River	Rhyolite	Kumola	784 ± 5
TS-1180	47°55′32.0″	66°16′13.01″	Baikonur River	Trachyrhyolite	Aktass	**797 ± 4**
U-9003	48°02′52.59″	66°19′15.04″	Aktass	Alkali granite	Aktass	**791 ± 7**

Age estimates indicated in bold were obtained by the authors [9, 22].

sured by the traditional technique described in [70]. The intensity of the primary beam of molecular negatively charged oxygen ions was ~2.5–4 nA; the spot (crater) diameter was ~15 × 10 μm. The data we obtained were processed using the SQUID [43] and ISOPLOT [42] software.

THE DATA OF THE U–Pb ISOTOPE–GEOCHRONOLOGICAL STUDIES

Complexes of the Dyusembai Association

Sample U-1103 (47°46′34.80″ N; 66°31′52.10″ E) was collected from rhyolite in the section in the upper reaches of the Dyusembai River to estimate the age of felsic volcanic rocks of the Dyusembai Formation (Table 1).

Accessory zircon was represented by euhedral crystals of prismatic and tabular habit, 50–200 μm in size, with an elongation factor of 2 to 4. The crystals were characterized by clear igneous zoning (Fig. 7).

The U–Pb geochronological studies were performed for 14 zircon crystals. The concordant age calculated from the $^{206}Pb/^{238}U$ ratio was 836 ± 6 Ma (Fig. 8a; Table 2).

Estimates of the age of detrital zircon grains were previously obtained for sheared volcanic–sedimentary felsic rocks of the Dyusembai Formation in the upper reaches of the Dyusembay River (Fig. 3, Sample M-12-13). They are dominated by subhedral crystals with clear igneous zoning, aged in the range of 840–1010 Ma with pronounced maxima at 846 and 904 Ma. There are a few rounded zircon grains with poorly expressed igneous zoning and ages of 1600–2200 Ma, as well [4].

To estimate the ages of rocks of the Zhaunkar Formation, Sample U-1671 (47°22′57.10″ N; 66°22′56.70″ E) was collected from trachydacite on the right bank of the Akyrlysai River (Table 1). Accessory zircon is represented by euhedral crystals of a prismatic, dipyramidal, and less commonly, a tabular habit, 100–200 μm in size, with an elongation factor of 2 to 4 (Fig. 7).

The crystals are characterized by clear igneous zoning. The U–Th–Pb geochronological studies were carried out for 19 zircon crystals. The concordant age calculated from the $^{206}Pb/^{238}U$ ratio was 823 ± 5 Ma (Fig. 8b, Table 2).

Thus, the data we obtained indicate that the age of the felsic volcanic rocks of the Dyusembai and Zhaunkar formations coincides within the error (825–830 Ma). Taking into account the close structure and compositional patterns of the rocks, their assignment to different formations is most likely explained by confinement to several tectonic plates occupying different structural positions.

An age estimate of 829 ± 10 Ma was previously obtained for granitoids of the North Sarysai Massif of the Zhaunkar Formation [9] (Fig. 4, Sample U-1331).

Complexes of the Aktass Association

A rhyolite sample (U-1349; 47°50′31.29″ N; 66°40′38.63″ E) was collected on the left bank of the Bereke River in order to estimate the age of felsic volcanic rocks from the upper part of the Kumola Formation section (Table 1). Accessory zircon is represented by euhedral crystals of a short prismatic, dipyramidal, and less commonly tabular habit, 80–200 μm in size, with an elongation factor of 1 to 2.

The crystals are characterized by clear igneous zoning (Fig. 7). The U–Pb geochronological studies were carried out for 15 zircon crystals. The concordant age calculated from the $^{206}Pb/^{238}U$ ratio was 784 ± 5 Ma (Fig. 8c, Table 2).

The ages of crystallization were previously estimated for volcanic rocks of the Koksui Group (Aktass Formation) and intruding granitoids of the Aktass Formation as 794 ± 3 Ma and 791 ± 7 Ma, respectively [23].

The morphological patterns of the studied zircon crystals indicate their igneous origin and the obtained age estimates reflect the age of crystallization of igneous rocks of the Dyusembai and Aktass associations. Based on the analysis of the data, we believe that the

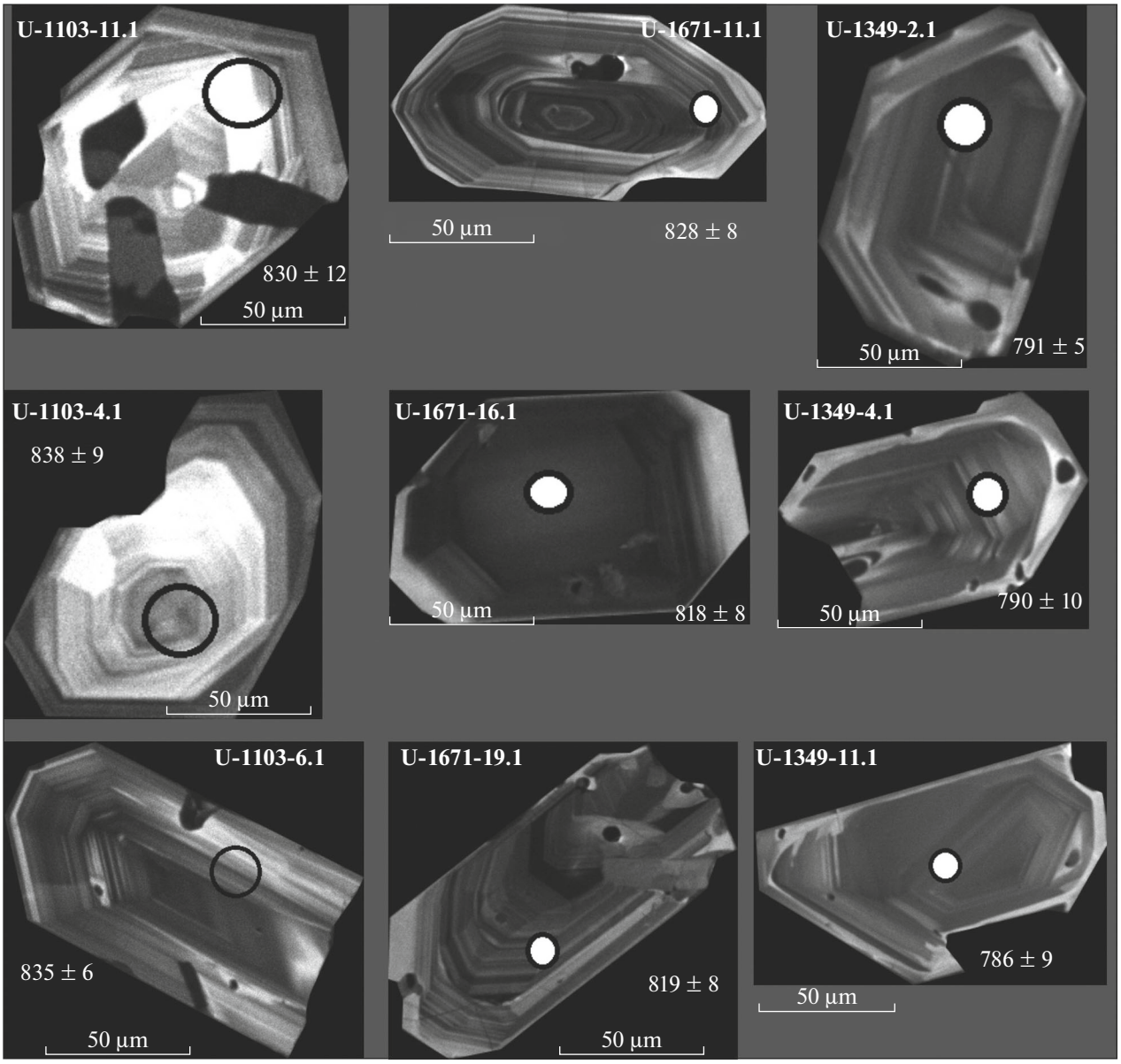

Fig. 7. CL images of studied zircons from felsic volcanic rocks of the Dyusembai (U-1103), Zhaunkar (U-1671), and Kumolin (U-1349) formations. The dated sites (circles) and concordant ages calculated from the $^{206}Pb/^{238}U$ ratio are shown.

formation of these associations occurred over close but different time intervals of the second half of the Tonian period in the Neoproterozoic: ~830 Ma (Dyusembai) and ~800–790 Ma (Aktass).

THE ISOTOPE–GEOCHEMICAL CHARACTERISTICS OF ROCKS OF THE VOLCANIC–PLUTONIC ASSOCIATIONS

Rocks of the Dyusembai association. According to the contents of SiO_2 and $Na_2O + K_2O$, the effusive rocks of the Dyusembai and Zhaunkar formations correspond to trachyte, trachydacite, and rhyolite, and the granitoids of the Zhaunkar Complex are close to the latter (Fig. 9, Table 3). The rocks are characterized by moderate and high alumina (ASI = 0.86–1.24) and high iron (FeO*/(FeO* + MgO) = 0.77–0.96) contents and low values of the agpaitic index (Ka = 0.63–0.97) (Fig. 10, Table 3).

The concentrations of TiO_2, Al_2O_3, FeO, MgO, and P_2O_5 decrease with an increase in the content of SiO_2 in rocks. There is no clear correlation between SiO_2 and alkalis, while the total of $Na_2O + K_2O$ decreases with increasing silica content (Fig. 11).

All rocks are characterized by a similar distribution of trace elements. With increasing SiO_2 content, the Eu anomaly appears in volcanic rocks and granite: from positive, in trachyte and trachydacite (Eu/Eu* =

0.9–1.6), to negative, in rhyolite (Eu/Eu* = 0.1–0.8) and granite (Eu/Eu* = 0.2–0.5). The depletion of rocks in Ba and Sr is observed in the same direction.

The rocks are characterized by enrichment in U, Th, Zr, Y and a differentiated REE distribution spectrum with $(La/Yb)_n$ = 3–23 (Fig. 12).

Rocks of the Aktass association. The effusive rocks of the Aktass, Lakbai, and Kumola formations plot into the fields of trachydacite and rhyolite on the SiO_2–$Na_2O + K_2O$ diagram, while granitoids of the Aktass complex, plot into the areas from trachyte to rhyolite (Fig. 9, Table 4). The rocks are characterized by moderate and high alumina (ASI = 0.92–1.34), high iron (FeO*/(FeO* + MgO) = 0.77–0.96) contents and an agpaitic index of Ka = 0.74–1 (Fig. 10, Table 4). An increase in the SiO_2 content in rocks is accompanied by a decrease in the concentrations of TiO_2, Al_2O_3, FeO, MgO, P_2O_5, Na_2O and an increase in K_2O (Fig. 11).

Effusive rocks and granitoids have similar trace-element distribution patterns. With increasing SiO_2 content, the rocks become depleted in Eu, Ba, and Sr. They are characterized by enrichment in U, Th, Zr, Y and a differentiated REE distribution spectrum with $(La/Yb)_n$ = 4–15 (Fig. 13).

Volcanic rocks of the Aktass Formation and granitoids of the Aktass Complex are characterized by wide variations in εNd (from +1.4 to –4.9) and model age of tNd(DM) = ~1.31–1.76 Ga) (Fig. 14, Table 5).

Granitoids of the Zhaunkar Complex are characterized by a negative εNd value (–11) and Early Precambrian model age (tNd(DM) = ~2.5 Ga) (Fig. 14, Table 5).

DISCUSSION OF THE RESULTS

We performed geological, geochronological, and isotope–geochemical studies, which allowed us to identify two Neoproterozoic (Late Tonian) volcanic–plutonic associations in the western part of the Southern Ulutau (Maityubinsk Zone), including the formations of felsic volcanic rocks and granitoids, namely the Dyusembai (~830 Ma) and Aktass (800–790 Ma).

The Environments of the Formation and Provenances of Rocks

The volcanic rocks and granitoids of different ages have similar patterns of the chemical composition characteristic of A-type granite. They mainly belong to the mid- and high-alumina, ferruginous series

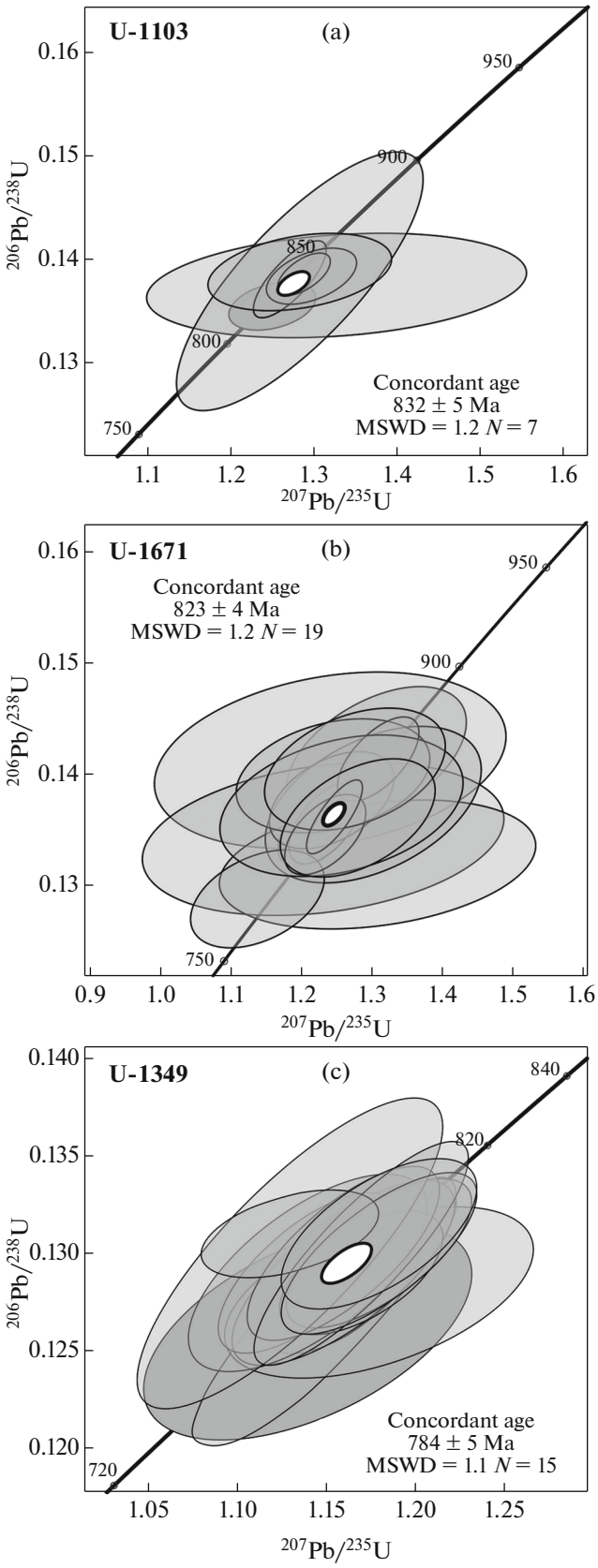

Fig. 8. The diagram with concordia for zircons of the Dyusembai, Zhaunkar, and Kumolin formations. (a) Sample U-1103, zircons from rhyolite of the Dyusembai Formation; (b) Sample U-1671, zircon from trachydacite of the Zhaunkar Formation; (c) Sample U1349, zircon from rhyolite of the Kumola Formation.

Table 2. The results of U–Pb geochronological studies of accessory zircons

Analysis no.	^{206}Pbc %	Concentration, ppm			Isotope ratios				Rho	Age, Ma	
		^{206}Pb*	U	Th	^{232}Th/^{238}U	^{207}Pb*/^{206}Pb*	^{206}Pb*/^{238}U	^{207}Pb*/^{235}U		^{206}Pb/^{238}U	^{207}Pb/^{206}Pb
U-1671											
1.1	0.00	15	128	163	1.32	0.0654 ± 1.5	0.1364 ± 1.2	1.231 ± 1.9	0.62	824 ± 9	788 ± 32
10.1	0.07	19.5	161	169	1.09	0.0672 ± 1.4	0.1413 ± 1.1	1.308 ± 1.8	0.60	852 ± 9	843 ± 30
11.1	0.04	26.3	223	286	1.32	0.0666 ± 1.2	0.1370 ± 1.0	1.258 ± 1.6	0.66	828 ± 8	825 ± 25
12.1	0.04	33.2	285	225	0.82	0.0664 ± 1.1	0.1353 ± 1.1	1.238 ± 1.5	0.70	818 ± 8	819 ± 23
13.1	0.00	2.76	23	23	1.04	0.0668 ± 3.5	0.1416 ± 1.8	1.305 ± 4.0	0.46	854 ± 15	833 ± 74
14.1	0.02	59.3	507	312	0.64	0.0664 ± 0.8	0.1361 ± 1.0	1.246 ± 1.3	0.77	823 ± 8	818 ± 17
15.1	0.81	2.09	18	18	1.03	0.0666 ± 8.2	0.1341 ± 2.1	1.230 ± 8.5	0.25	811 ± 16	825 ± 170
16.1	0.07	19.3	166	165	1.03	0.0654 ± 1.5	0.1353 ± 1.1	1.220 ± 1.8	0.59	818 ± 8	787 ± 31
17.1	0.88	3.19	28	36	1.34	0.0719 ± 6.7	0.1318 ± 1.8	1.307 ± 7.0	0.26	798 ± 13	984 ± 140
18.1	0.00	1.83	16	15	0.97	0.0688 ± 4.3	0.1372 ± 2.1	1.301 ± 4.8	0.44	829 ± 17	892 ± 89
19.1	0.06	21.7	186	99	0.55	0.0660 ± 1.4	0.1355 ± 1.1	1.233 ± 1.7	0.62	819 ± 8	806 ± 29
2.1	0.22	5.71	52	74	1.49	0.0641 ± 3.1	0.1287 ± 1.4	1.137 ± 3.4	0.41	781 ± 10	744 ± 66
3.1	0.08	17.2	149	146	1.02	0.0665 ± 1.6	0.1345 ± 1.1	1.233 ± 1.9	0.58	814 ± 9	821 ± 33
4.1	0.18	7.29	62	63	1.06	0.0655 ± 2.6	0.1376 ± 1.3	1.242 ± 2.9	0.45	831 ± 10	790 ± 55
5.1	0.44	5.17	43	43	1.03	0.0645 ± 4.3	0.1398 ± 1.5	1.244 ± 4.5	0.33	843 ± 12	759 ± 90
6.1	0.49	2.57	22	23	1.10	0.0664 ± 5.3	0.1371 ± 1.9	1.256 ± 5.6	0.33	828 ± 15	821 ± 110
7.1	0.30	4.35	36	44	1.25	0.0659 ± 3.8	0.1404 ± 1.6	1.275 ± 4.1	0.38	847 ± 12	803 ± 79
8.1	0.00	3.53	30	42	1.45	0.0682 ± 3.1	0.1360 ± 1.6	1.279 ± 3.5	0.46	822 ± 13	875 ± 65
9.1	0.77	1.78	15	13	0.90	0.0638 ± 7.9	0.1412 ± 2.3	1.240 ± 8.2	0.28	851 ± 18	736 ± 170
U-1103											
5.1	0.00	44	378	182	0.50	0.0670 ± 1.6	0.1355 ± 0.7	1.250 ± 1.7	0.41	819 ± 5	835 ± 33
11.1	0.00	4.78	41	62	1.57	0.0701 ± 6.8	0.1375 ± 1.5	1.327 ± 7.0	0.21	830 ± 12	929 ± 1409
2.1	0.00	29	245	291	1.23	0.0675 ± 2.9	0.1379 ± 3.7	1.284 ± 4.7	0.79	833 ± 29	854 ± 59
10.1	0.00	81.1	684	691	1.04	0.0667 ± 0.9	0.1381 ± 1.1	1.271 ± 1.4	0.79	834 ± 9	829 ± 18
6.1	0.00	32.2	271	523	1.99	0.0680 ± 1.5	0.1384 ± 0.8	1.297 ± 1.7	0.48	835 ± 6	868 ± 31
3.1	0.00	128	1075	558	0.54	0.0674 ± 0.8	0.1386 ± 0.6	1.288 ± 1.0	0.64	837 ± 5	849 ± 16
4.1	0.00	9.7	81	169	2.15	0.0670 ± 3.3	0.1388 ± 1.1	1.283 ± 3.5	0.33	838 ± 9	839 ± 68
U-1349											
15.1	1.03	79.3	732	766	1.08	0.0653 ± 2.8	0.1261 ± 1.6	1.136 ± 3.3	0.53	766 ± 13	785 ± 58
13.1	0.00	73.9	678	435	0.66	0.0659 ± 1.3	0.1268 ± 2.2	1.153 ± 2.6	0.86	770 ± 16	804 ± 27
5.1	0.04	108	976	821	0.87	0.0657 ± 1.1	0.1284 ± 0.9	1.162 ± 1.5	0.64	779 ± 7	796 ± 24
12.1	1.18	90.2	817	821	1.04	0.0664 ± 2.6	0.1284 ± 1.4	1.175 ± 3.0	0.46	779 ± 10	818 ± 55
7.1	0.27	94.5	855	714	0.86	0.0656 ± 1.5	0.1287 ± 1.5	1.165 ± 2.2	0.70	780 ± 11	795 ± 32
6.1	0.19	117	1058	944	0.92	0.0642 ± 1.3	0.1292 ± 1.3	1.143 ± 1.8	0.71	783 ± 10	747 ± 27
1.1	0.25	69.5	626	470	0.78	0.0638 ± 1.8	0.1292 ± 1.6	1.137 ± 2.4	0.66	783 ± 12	736 ± 38
3.1	0.00	78.1	703	572	0.84	0.0657 ± 1.3	0.1293 ± 1.1	1.172 ± 1.6	0.62	784 ± 8	798 ± 27
11.1	0.03	80.9	726	579	0.82	0.0662 ± 1.3	0.1297 ± 1.2	1.183 ± 1.8	0.69	786 ± 9	811 ± 27
14.1	0.03	78.9	706	518	0.76	0.0645 ± 1.3	0.1300 ± 1.4	1.156 ± 1.9	0.74	788 ± 11	759 ± 27
9.1	0.34	79.8	714	517	0.75	0.0633 ± 1.8	0.1300 ± 2.5	1.134 ± 3.1	0.81	788 ± 19	717 ± 39
8.1	0.05	109	976	878	0.93	0.0651 ± 1.2	0.1300 ± 1.8	1.167 ± 2.1	0.84	788 ± 13	777 ± 24
4.1	0.12	87.2	778	697	0.92	0.0659 ± 1.3	0.1304 ± 1.3	1.185 ± 1.9	0.70	790 ± 10	803 ± 28
2.1	0.25	88.8	791	692	0.90	0.0629 ± 1.6	0.1306 ± 0.7	1.134 ± 1.8	0.41	791 ± 5	706 ± 34
10.1	0.15	78.8	700	495	0.73	0.0653 ± 1.5	0.1310 ± 1.2	1.179 ± 1.9	0.62	793 ± 9	784 ± 31

^{206}Pbc, common Pb; ^{206}Pb*, radiogenic Pb; Rho, coefficient of error correlation ^{207}Pb/^{235}U–^{206}Pb/^{238}U. Error of isotope ratio measurements (%) is given at the level of 1σ.

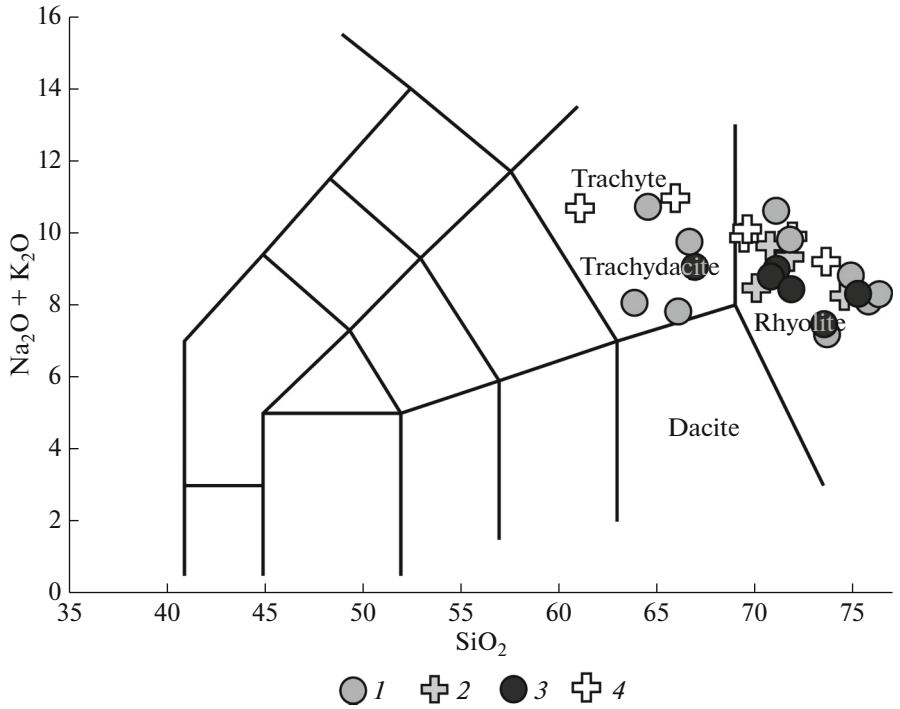

Fig. 9. The SiO_2–$Na_2O + K_2O$ diagram for igneous rocks of the Dyusembai and Aktass volcanic–plutonic associations, after [38]. (*1*) Effusive rocks of the Dyusembai and Zhaunkar formations; (*2*) granitoids of the Zhaunkar Complex; (*3*) effusive rocks of the Aktass and Kumola formations; (*4*) granitoids of the Aktass Complex.

(Fig. 10). According to the relationships of $CaO/(FeO^* + MgO + TiO_2)$ vs. $CaO + Al_2O_3$ and FeO^*/MgO vs. $Zr + Nb + Ce + Y$, the least-differentiated varieties plot in the field of A-type granite, which is supported by the enrichment of rocks in U, Th, Zr, Y and slight depletion in Nb and Ta against the background of a sharp depletion in Ba, Sr, P, Eu, and Ti [25, 67] (Figs. 14, 15). The calculated temperatures of saturation of their parent melts with Zr (average T_{Zr} of 800°C (~830 Ma) and 840°C (~790 Ma)) indicate the high-temperature mode of their formation, which is a characteristic feature of Fe-rich A-type granite, while the Rb–Y + Nb relationships suggest the formation of melts in an intraplate extension setting (Fig. 15) [47, 50, 69].

The linear dependences between SiO_2 and rock-forming oxides in the rocks of both associations are the result of fractional crystallization.

A decrease in $Na_2O + K_2O$ content with increase in SiO_2, positive linear correlations between Ba and Sr, and negative ones between Ba and Rb indicate the removal of alkali feldspar from the melt (Fig. 11).

Fractionation of alkali feldspar seems to be the key factor in the evolution of A-type acid melts [25, 26], which is supported by the depletion of the most felsic varieties in Eu/Eu*, Ba, and Sr.

The different behavior of Zr relative to SiO_2 suggests the removal of accessory minerals (zircon) in the rocks of the Dyusembai (~830 Ma) association and their accumulation in the volcanic rocks and granite of the Aktass (800–790 Ma) association at the final stages of melt differentiation.

The negative correlation between SiO_2 and Zr is indicative of zircon fractionation. Correspondingly, the calculated temperature of saturation with zircon, 740–850°C, is lower than that of the initial melt. These data characterize volcanic rocks and granitoids as products of the evolution of melts with similar compositions.

Acid igneous rocks with A-type characteristics are usually considered as a result of melting of rocks of the continental crust or mantle–crust interaction, as well as rocks of the mantle origin [16, 19–21, 25, 26, 29, 64]. In the last two versions, it is assumed that felsic rocks are differentiates of mantle melts or differentiates that have experienced assimilation by crustal melts. In these cases, felsic varieties usually associate with basalt, trachybasalt, and, more rarely, rocks of intermediate composition, forming bimodal series [15].

Felsic volcanic rocks and their plutonic analogs in such associations have an alkaline sialic composition. The presence of dark-colored alkaline minerals and a high agpaitic index are characteristic of alkaline rhyolite, namely, comendite and pantellerite [47]. At the same time, rocks of associations with different silica content have the same variations in the Nd isotope composition, close to the mantle one.

The absence of mafic igneous rocks with ages of ~830 and ~790 Ma at the modern erosion level of the Maityubinsk Zone, the presence of biotite and horn-

Table 3. The concentrations of major (wt %) and trace (ppm) elements in effusive and plutonic rocks of the Dyusembai association

Component	Dyusembai Formation				Zhaunkar Formation							Zhaunkar granite complex			
	U-1102	U-1102/1	U-1103	U-1104	U-1666	U-1667	U-1668	U-1670	U-1671	U-1326	U-9005	U-1325	U-1331	U-9006	U-9008
SiO_2 (%)	63.92	66.11	76.98	73.68	66.68	77.89	71.79	75.78	64.57	74.88	71.09	70.08	74.56	71.77	70.79
TiO_2 (%)	0.61	0.41	0.08	0.14	0.38	0.15	0.35	0.22	0.42	0.12	0.12	0.22	0.24	0.20	0.22
Al_2O_3 (%)	17.89	17.32	12.03	14.44	15.41	11.03	13.94	11.80	16.25	12.83	15.54	15.10	12.54	14.86	15.12
Fe_2O_3 (%)	1.24	0.19	0.10	0.20	3.12	1.37	2.30	1.83	3.25	1.80	0.38	1.63	1.04	1.29	0.58
FeO (%)	2.87	3.55	1.26	2.07	0.14	0.12	0.18	0.50	0.46	0.20	1.15	1.32	1.29	1.20	1.84
MnO (%)	0.06	0.05	0.01	0.04	0.10	0.05	0.05	0.04	0.12	0.03	0.04	0.06	0.04	0.02	0.04
MgO (%)	1.22	0.16	0.01	0.19	0.42	0.27	0.33	0.33	0.60	0.12	0.31	0.82	0.35	0.43	0.61
CaO (%)	3.16	2.56	0.68	1.11	2.56	1.03	0.52	0.58	2.13	0.52	0.45	0.71	0.81	0.42	0.55
K_2O (%)	3.73	3.46	4.97	1.72	4.86	3.42	6.00	4.77	5.88	4.98	5.76	5.21	4.78	4.92	4.64
Na_2O (%)	4.43	4.36	3.38	5.47	4.89	3.70	3.81	3.33	4.84	3.84	4.85	3.26	3.47	4.41	5.00
P_2O_5 (%)	0.20	0.10	0.01	0.04	0.11	0.04	0.08	0.06	0.18	0.01	0.03	0.08	0.07	0.06	0.06
LOI (%)	0.52	1.21	0.38	0.87	1.32	0.91	0.64	0.71	1.26	0.65	0.58	1.37	0.68	0.96	0.90
Total	*99.85*	*99.48*	*99.89*	*99.97*	*99.98*	*99.99*	*99.98*	*99.94*	*99.95*	*99.98*	*100.29*	*99.86*	*99.86*	*100.54*	*100.34*
$Na_2O + K_2O$	8.16	7.82	8.35	7.19	9.75	7.13	9.81	8.10	10.71	8.82	10.61	8.46	8.24	9.33	9.64
K_2O/Na_2O	0.84	0.79	1.47	0.31	0.99	0.92	1.57	1.43	1.21	1.30	1.19	1.60	1.38	1.12	0.93
(Na + K)Al	0.63	0.63	0.91	0.75	0.86	0.89	0.92	0.90	0.88	0.91	0.91	0.73	0.87	0.85	0.88
FeO*	3.99	3.72	1.35	2.25	2.94	1.36	2.25	2.15	3.38	1.82	1.49	2.79	2.23	2.36	2.36
FeO*/(FeO* + MgO)	0.77	0.96	0.99	0.92	0.88	0.83	0.87	0.87	0.85	0.94	0.83	0.77	0.87	0.85	0.79
ASI	1.06	1.12	0.99	1.13	0.86	0.95	1.02	1.01	0.90	1.02	1.04	1.24	1.02	1.12	1.07
MALI	5.00	5.26	7.67	6.08	7.19	6.10	9.29	7.52	8.59	8.30	10.17	7.75	7.44	8.91	9.09
Sc	–	–	–	–	8.29	2.62	7.55	4.45	4.61	–	3.41	–	–	4.57	4.6
V	39.90	22.30	7.01	8.82	15.52	3.26	9.84	12.80	9.14	6.38	11.61	18.00	14.70	9.27	9.3
Cr	23.30	24.90	23.00	22.70	9.91	20.63	15.07	5.27	2.77	54.50	19.76	23.60	22.00	14.35	14.4
Co	4.56	3.18	0.58	0.95	1.57	1.08	1.78	1.39	1.84	0.73	2.11	2.86	2.68	3.36	3.4
Ni	12.80	14.30	8.09	13.90	6.13	11.19	10.24	3.73	1.57	23.10	8.62	8.75	9.25	15.44	15.4
Cu	7.76	10.90	8.94	11.80	2.88	1.71	2.59	1.18	3.02	19.40	12.50	15.50	13.20	19.71	19.7
Zn	61.70	81.00	65.20	59.50	29.90	20.93	30.34	26.44	53.04	81.70	38.97	128	64.60	34.85	34.8
Ga	17.40	20.30	18.40	16.70	14.01	7.80	12.48	15.56	13.82	19.20	14.43	18.70	16.80	12.54	12.5
Rb	90.90	104	218	48.70	74.96	85.95	123.04	204.44	85.91	174	122.87	185	137	88.19	88.2
Sr	574	378	28.30	37.10	249.26	124.54	131.43	59.90	254.51	10.60	67.80	79.60	113	81.67	81.7
Y	25.70	28.00	51.50	26.70	21.30	19.19	27.87	80.20	21.76	40.50	21.30	26.30	37.10	31.79	31.8

Table 3. (Contd.)

Component	Dyusembai Formation				Zhaunkar Formation							Zhaunkar granite complex			
	U-1102	U-1102/1	U-1103	U-1104	U-1666	U-1667	U-1668	U-1670	U-1671	U-1326	U-9005	U-1325	U-1331	U-9006	U-9008
Zr	280	335	93.80	121	344.46	88.23	234.07	201.40	468.64	242	127.72	176	279	138.32	138
Nb	19.00	20.10	24.50	17.10	11.96	12.84	16.84	19.27	11.80	22.10	17.92	17.50	17.80	18.10	18.1
Mo	0.86	0.68	1.18	0.71	0.33	0.42	0.60	0.69	0.61	1.07	3.88	0.86	1.96	1.62	1.6
Cs	3.05	2.75	2.28	1.01	2.32	2.62	1.59	1.60	1.48	2.72	0.78	1.33	0.54	0.42	0.42
Ba	1320	1080	90.40	269	4307.20	840.30	1829.64	338.97	2917.13	63.30	438.38	444	888	498.95	499
La	58.90	62.40	18.10	49.80	65.53	44.86	80.70	99.41	84.86	80.60	21.79	47.40	71.90	34.07	34.1
Ce	109	113	44.40	97.50	114.17	85.08	141.35	196.93	149.94	150	48.83	81.30	137	68.03	68.0
Pr	12.50	13.00	6.99	11.40	11.23	8.27	15.75	20.36	14.39	16.90	6.01	8.77	15.10	7.84	7.8
Nd	46.10	49.20	32.70	44.60	43.03	30.94	54.85	68.86	54.29	63.30	23.52	33.40	51.00	29.81	29.8
Sm	7.61	7.41	10.80	7.34	6.60	5.28	8.88	12.69	7.52	10.70	4.95	5.80	8.46	5.93	5.9
Eu	2.07	2.05	0.29	0.58	3.05	0.67	1.92	0.78	3.26	0.12	0.41	0.79	1.12	0.47	0.47
Gd	6.83	6.18	11.90	6.60	4.98	4.04	6.81	11.05	5.38	9.10	4.62	4.87	7.45	6.00	6.0
Tb	0.86	0.91	2.07	0.85	0.70	0.61	0.98	1.92	0.77	1.26	0.82	0.70	1.04	1.05	1.1
Dy	5.16	5.31	13.10	5.27	3.97	3.49	5.57	11.81	4.27	7.30	4.32	4.55	6.32	5.49	5.5
Ho	0.99	1.07	2.20	0.93	0.77	0.67	1.04	2.52	0.83	1.47	0.88	0.86	1.40	1.09	1.1
Er	2.45	2.72	4.88	2.68	2.32	2.03	3.08	7.49	2.53	4.11	2.67	2.58	3.53	3.48	3.5
Tm	0.39	0.44	0.71	0.43	0.33	0.28	0.44	1.05	0.37	0.63	0.38	0.45	0.66	0.50	0.50
Yb	2.28	2.85	4.21	2.33	2.19	2.00	2.97	6.55	2.51	3.89	2.79	2.43	3.93	3.36	3.4
Lu	0.33	0.38	0.50	0.31	0.34	0.29	0.44	0.90	0.38	0.58	0.41	0.39	0.50	0.50	0.50
Hf	7.43	8.07	5.70	5.18	7.24	3.01	6.14	6.33	9.34	7.79	4.87	5.30	8.07	4.97	5.0
Ta	1.23	1.41	2.04	1.39	0.66	0.81	0.98	1.54	0.66	1.64	1.42	1.59	1.30	1.48	1.5
W	1.14	1.32	1.12	1.05	1.79	0.66	0.87	0.85	1.14	1.22	0.88	1.76	1.08	0.53	0.53
Pb	42.90	35.80	51.30	18.80	12.26	7.64	12.73	23.04	11.74	34.00	12.80	128	42.30	14.36	14.4
Th	11.70	12.50	15.70	15.00	6.28	9.85	9.86	38.98	5.09	17.20	9.61	18.40	20.40	14.36	14.4
U	1.78	1.39	2.80	1.49	1.11	1.11	1.69	2.73	1.29	1.53	1.47	2.89	2.35	0.82	0.82
Ti	3655.73	2457.13	479.44	839.02	2273.74	910.94	2100.55	1299.28	2543.43	702.98	700.08	1309.47	1461.69	1202.65	1305.93
P	873.20	436.60	43.66	174.64	458.43	166.78	332.25	249.30	764.05	52.39	115.86	370.24	296.01	269.08	274.30
$(La/Yb)_n$	17.44	14.78	2.90	14.43	20.16	15.13	18.35	10.25	22.78	13.99	5.27	13.17	12.35	6.84	6.80
Eu/Eu*	0.88	0.93	0.08	0.25	1.63	0.44	0.75	0.20	1.56	0.04	0.26	0.45	0.43	0.24	0.23
T°C	820	850	741	769	819	734	815	807	849	823	761	807	837	777	770

FeO* = 0.9 FeO + F_2O_3; ASI = (Al/(Ca–1.67 P + Na + K)); MALI = (Na_2O + K_2O–CaO); *T*°C is the temperature of saturation in Zr obtained using the thermometer, after [70].

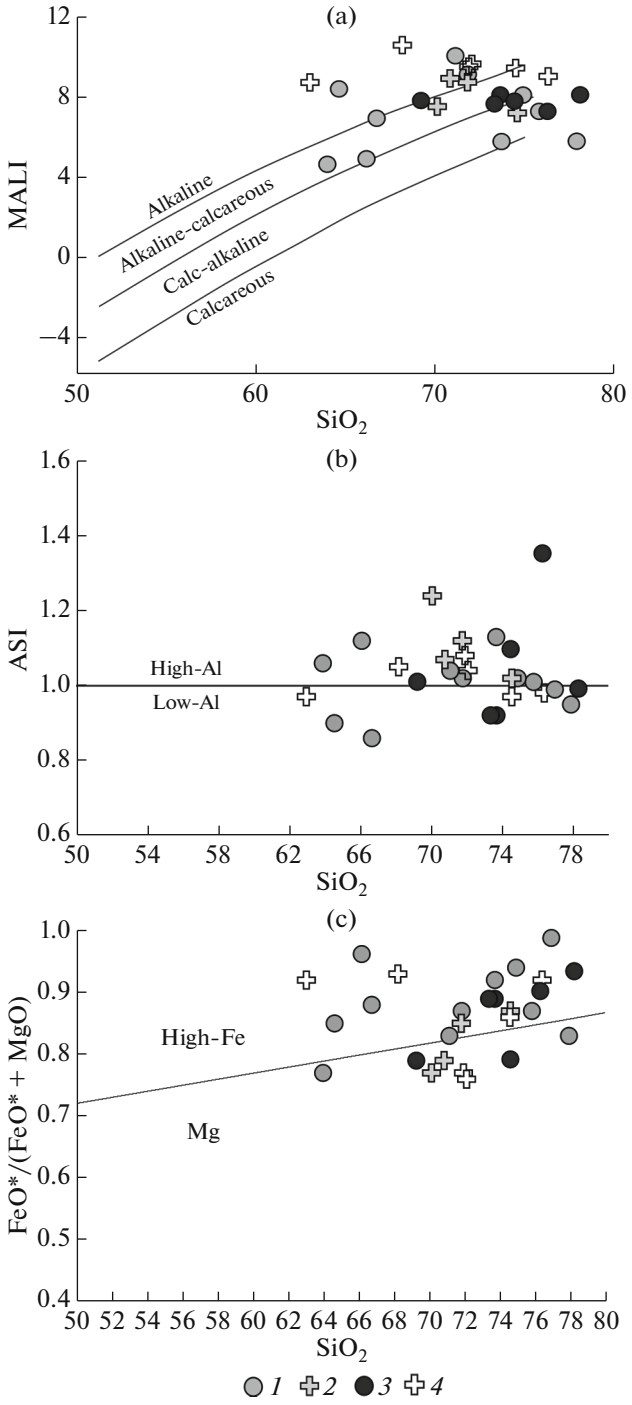

Fig. 10. Diagrams for igneous rocks of the Dyusembai and Aktass volcanic–plutonic associations, after [28]. (a) SiO_2–MALI ($Na_2O + K_2O$–CaO); (b) SiO_2–ASI (Al/(Ca–1.67P + Na + K)); (c) SiO_2–FeO*/(FeO* + MgO). (*1*) Effusive rocks of the Dyusembai and Zhaunkar formations; (*2*) granitoids of the Zhaunkar Complex; (*3*) effusive rocks of the Aktass and Kumola formations; (*4*) granitoids of the Aktass Complex.

blende among the mafic minerals of volcanic rocks and granitoids indicate the absence of a direct relationship between the formation of the latter and the evolution of basic melts.

Fig. 11. Variation diagrams of some major and trace elements. (a) SiO_2–TiO_2; (b) SiO_2–Al_2O_3*; (c) SiO_2–FeO; (d) SiO_2–MgO; (e) Ba–Rb; (f) Ba–Sr; (g) SiO_2–Zr. (*1*) Dyusembai association; (*2*) Aktass association.

The petrogeochemical characteristics of effusive rocks and granite are comparable with the melting products of continental crust rocks [29]. Variations of petrogenic and trace elements in effusive rocks and granitoids of the Dyusembai association with an age of ~830 Ma, as well as a negative between of SiO_2 and Zr, which indicates fractionation of zircon, allow us to consider trachyte and trachydacite as the least differentiated varieties and accept their T_{Zr} (~820–850°C) value as that close to the temperatures of the initial melt (see Fig. 11).

The positive correlation of SiO_2 and Zr in igneous rocks of the Aktass association with an age of ~790 Ma indicates the accumulation of zircon at the final stages of melt fractionation and allows us to accept T_{Zr} (~790–830°C) value of granitoids of the Aktass Complex as that close to the temperatures of the original melt (Fig. 11).

The absence of xenogenic cores in accessory zircons allows us to consider the obtained Zr saturation temperatures as the minimum ones [44]. Based on this, the melting temperatures were more than 800°C, which refers these formations to the "hot" granite type [47].

The melts formed via metapelite source melting are characterized by high contents of K_2O and low concentrations of CaO, FeO*, and MgO. The enrichment in Rb against the background of depletion in Ba and Sr associates with the dehydration melting of muscovite, against the background of biotite stability and, most likely, the absence of plagioclase in the source.

The high iron content in trachyte, trachydacite, and granitoids of the Aktass Complex is more characteristic of the melting products of quartz–feldspar rocks represented by metatonalite and metagraywacke [29].

Melting of these substrates in the range of $P = 4$–8 kbar leads to the formation of mid-aluminous ferruginous melts due to the dehydration biotite melting [49, 59, 65]. The formation of clinopyroxene instead of orthopyroxene in restite at pressures of more than 8 kbar is accompanied by an increase in Mg and Al contents in melts (ASI = 1.4–1.6) [49].

Dehydration melting of biotite at a pressure of 5 kbar or more leads to the formation of garnet [59, 65]. The high content of HREEs and Y in the studied volcanic rocks and granitoids indicates the formation of melts at pressures of 5 kbar or less.

The participation of biotite in the formation of parental melts is supported by the high concentrations of Ba in effusive rocks and granitoids. At the same time, trachyte and trachydacite are enriched in Eu (Eu/Eu* = 0.9–1.6) and Sr (255–574 ppm), which suggests the involvement of plagioclase in melting.

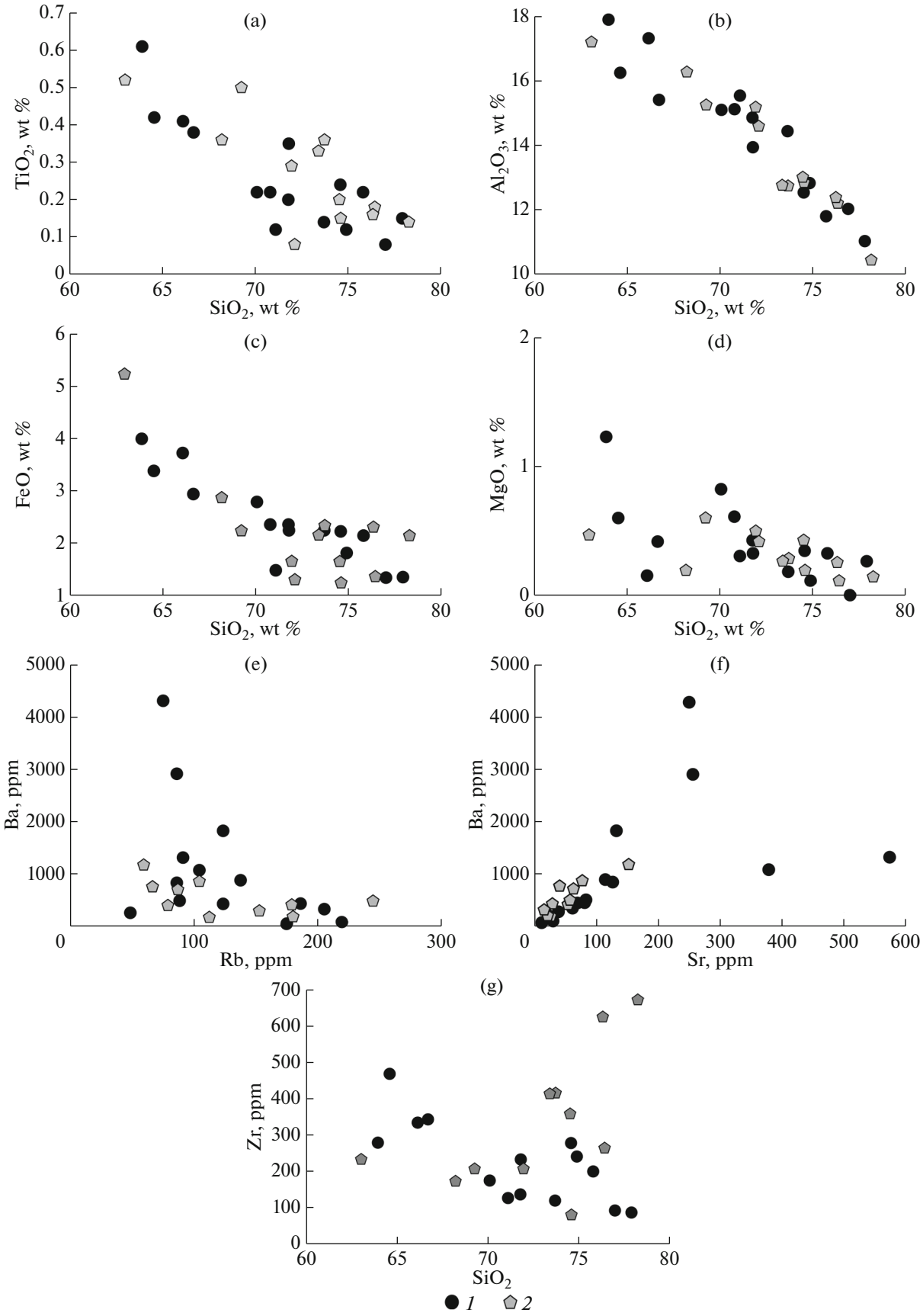
(a)
TiO2, wt %
SiO2, wt %
(b)
Al2O3, wt %
SiO2, wt %
(c)
FeO, wt %
SiO2, wt %
(d)
MgO, wt %
SiO2, wt %
(e)
Ba, ppm
Rb, ppm
(f)
Ba, ppm
Sr, ppm
(g)
Zr, ppm
SiO2
1
2

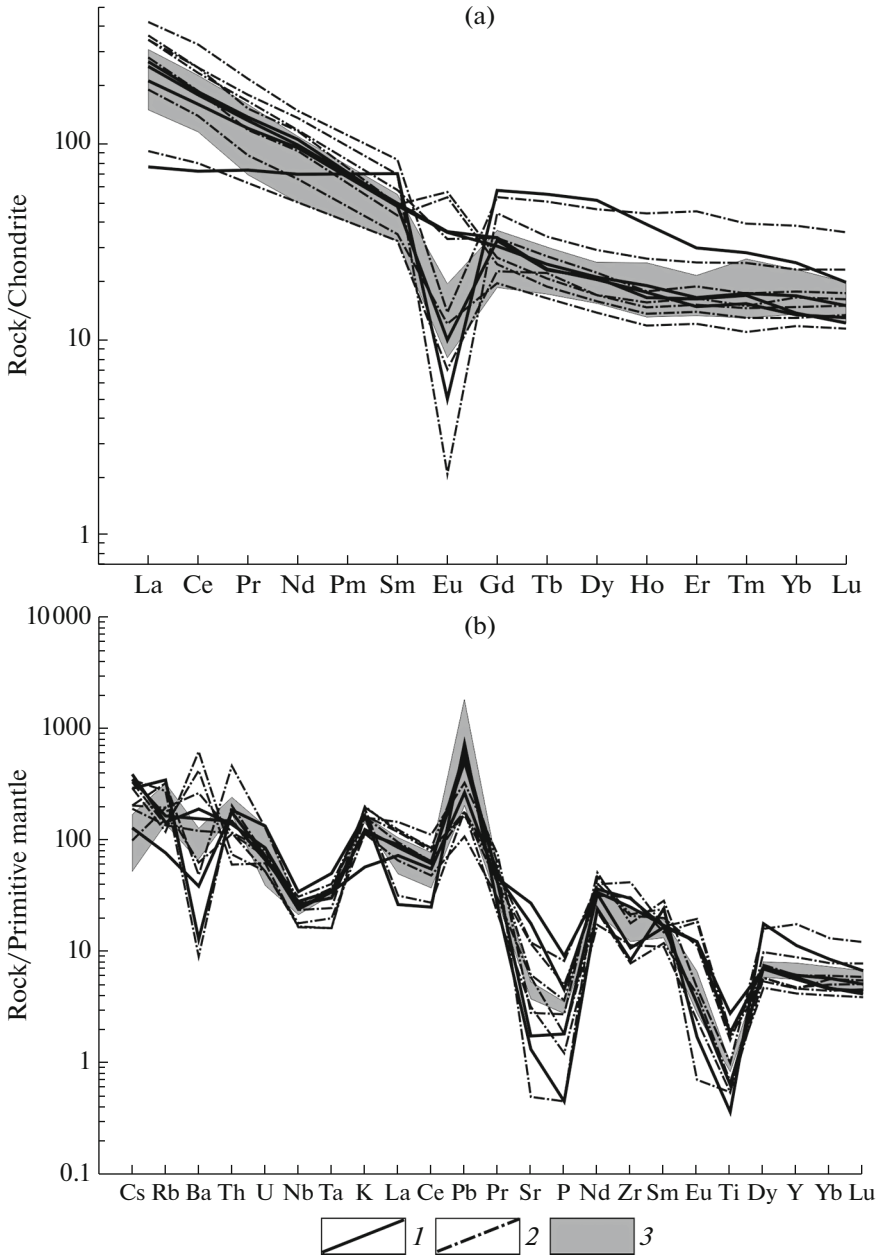

Fig. 12. The distribution spectra of rare and rare-earth elements in the rocks of the Dyusembai association, after [61]. (a) Chondrite-normalized; (b) normalized to the composition of the primitive mantle. (*1*) Effusive rocks of the Dyusembai Formation; (*2*) effusive rocks of the Zhaunkar Formation; (*3*) granitoids of the Zhaunkar Complex.

In turn, the depletion of granitoids of the Aktass association in Eu (Eu/Eu* = 0.01–0.5) and Sr (24–151 ppm) may indicate the stability of plagioclase.

Thus, the formation of parental melts for effusive and plutonic rocks of both associations occurred via dehydration melting of metatonalite (metagraywacke). Differences in the composition of liquidus phases may reflect certain differences in the sources of melts, which is also confirmed by the isotope-geochemical characteristics.

The low Nd isotope compositions of granitoids of the Zhaunkar Complex (~830 Ma), εNd(T) from –10.8 to –11, T(Nd)(DM) = 2.5, indicate their formation via partial melting of the Early Precambrian continental crust.

Variations in the Nd isotope composition in effusive rocks and granitoids with an age of ~790 Ma (~830 Ma), εNd(T) from –4.9 to +1.4, T(Nd)(DM) = 1.36–1.86, may reflect the addition of juvenile mantle material to the Early Precambrian crustal source (i) or melting of a heterogeneous source composed of rocks with different crustal prehistory (ii). The latter variant seems more plausible, since the calculation of the two-component mixing model [36] showed a significant contribution (up to 80%) of the mantle material to the

Table 4. The concentrations of major (wt %) and trace (ppm) elements in effusive and plutonic rocks of the Aktass association

Component	Kumola Formation			Aktass Formation			Aktass granite complex					
	U-1349	U-1328	U-1329	U-9001	TS-1177	TS-1180	U-9002	U-9003	TS-1175	TS-1176	TS-1179	U-1672
SiO_2	74.51	78.24	76.31	69.25	73.71	73.39	71.94	72.11	68.20	63.00	76.41	74.58
TiO_2	0.20	0.14	0.16	0.50	0.36	0.33	0.29	0.08	0.36	0.52	0.18	0.15
Al_2O_3	13.01	10.44	12.38	15.25	12.74	12.76	15.18	14.59	16.27	17.20	12.20	12.85
Fe_2O_3	1.65	2.04	2.31	2.02	2.21	2.12	1.11	0.92	3.06	1.44	1.39	0.49
FeO	0.17	0.31	0.23	0.42	0.35	0.25	0.66	0.48	0.12	3.92	0.12	0.81
MnO	0.03	0.02	0.02	0.04	0.06	0.06	0.03	0.01	0.02	0.18	0.01	0.02
MgO	0.43	0.15	0.26	0.60	0.29	0.27	0.50	0.42	0.20	0.47	0.12	0.20
CaO	0.63	0.19	0.07	1.21	0.87	1.11	0.30	0.39	0.31	1.92	0.13	0.41
K_2O	5.28	6.01	5.48	3.13	4.40	4.33	4.56	5.60	5.27	5.46	5.07	6.60
Na_2O	3.08	2.24	1.91	5.89	4.56	4.42	5.26	4.46	5.65	5.18	4.09	3.26
P_2O_5	0.03	0.02	0.03	0.17	0.06	0.08	0.05	0.03	0.07	0.13	0.03	0.04
LOI (%)	0.96	0.16	0.82	1.23	0.34	0.85	0.77	1.56	0.46	0.16	0.26	0.51
Total	*99.98*	*99.97*	*99.98*	*99.71*	*99.95*	*99.97*	*100.66*	*100.65*	*99.99*	*99.59*	*100.00*	*99.91*
$Na_2O + K_2O$	8.36	8.25	7.39	9.02	8.96	8.75	9.82	10.06	10.92	10.64	9.16	9.86
K_2O/Na_2O	1.71	2.68	2.87	0.53	0.96	0.98	0.87	1.25	0.93	1.05	1.24	2.02
(Na + K)Al	0.83	0.98	0.73	0.86	0.96	0.94	0.90	0.92	0.92	0.84	1.00	0.97
FeO*	1.66	2.15	2.31	2.24	2.34	2.16	1.66	1.31	2.87	5.22	1.37	1.25
FeO*/(FeO* + MgO)	0.79	0.93	0.90	0.79	0.89	0.89	0.77	0.76	0.93	0.92	0.92	0.86
ASI	1.09	0.99	1.35	1.01	0.92	0.92	1.08	1.04	1.05	0.97	0.98	0.97
MALI	7.73	8.06	7.32	7.81	8.09	7.64	9.52	9.66	10.61	8.72	9.03	9.45
Sc	–	–	–	3.72	7.50	6.42	3.72	–	2.97	8.89	1.77	1.78
V	10.70	8.23	8.06	4.15	23.82	23.13	4.15	–	9.57	12.37	8.95	6.83
Cr	28.30	54.00	22.40	17.10	4.96	5.99	17.10	–	3.80	7.14	4.65	10.59
Co	1.06	0.87	0.93	1.57	1.25	1.34	1.57	–	0.49	1.03	0.84	0.86
Ni	10.20	21.30	8.12	6.43	2.87	4.64	6.43	–	1.44	3.43	1.92	6.63
Cu	5.90	14.80	18.50	7.84	4.59	4.24	7.84	–	4.42	6.00	2.84	1.72
Zn	55.10	72.10	78.90	39.12	43.05	18.82	39.12	–	19.41	131.21	21.78	17.36
Ga	18.50	23.20	24.70	14.65	18.62	18.07	14.65	–	30.24	27.94	18.03	14.70
Rb	178	179	152	66.50	104.05	86.80	66.50	–	78.76	59.42	111.80	242.77
Sr	27.30	19.60	13.80	39.05	75.79	61.53	39.05	–	52.62	150.83	24.47	55.92
Y	51.40	93.00	96.20	39.91	50.55	45.98	39.91	–	25.87	63.55	58.92	20.46

Table 4. (Contd.)

Component	Kumola Formation			Aktass Formation			Aktass granite complex					
	U-1349	U-1328	U-1329	U-9001	TS-1177	TS-1180	U-9002	U-9003	TS-1175	TS-1176	TS-1179	U-1672
Zr	359	672	625	207.52	416.06	413.94	207.52	–	173.99	234.32	265.35	81.46
Nb	21.30	33.40	29.10	12.26	20.11	20.02	12.26	–	26.14	28.11	13.47	13.88
Mo	0.71	0.97	0.68	2.21	1.78	0.46	2.21	–	1.21	0.84	0.55	1.08
Cs	1.15	0.54	1.28	1.06	1.08	0.66	1.06	–	0.25	0.60	0.44	1.12
Ba	420	192	303	762.16	864.53	707.63	762.16	–	406.20	1177.79	181.08	490.55
La	40.90	74.90	59.00	40.62	50.15	38.91	40.62	–	43.96	97.08	50.19	35.42
Ce	85.50	142	114	100.96	115.80	97.83	100.96	–	91.56	203.14	99.87	70.51
Pr	9.65	18.20	13.50	10.67	12.61	11.03	10.67	–	10.65	22.94	10.66	6.64
Nd	34.50	67.20	54.30	41.09	47.37	41.36	41.09	–	38.61	89.64	37.89	24.48
Sm	7.32	12.00	11.70	8.08	10.09	9.96	8.08	–	7.01	16.23	7.92	4.73
Eu	0.62	0.17	0.33	1.21	1.86	1.07	1.21	–	1.59	3.92	0.37	0.55
Gd	7.27	12.70	12.30	7.48	9.51	9.39	7.48	–	5.75	14.04	8.70	3.82
Tb	1.27	2.33	2.16	1.23	1.49	1.44	1.23	–	0.90	2.11	1.45	0.64
Dy	8.11	16.60	16.60	6.98	8.67	8.34	6.98	–	4.68	11.19	9.00	3.91
Ho	1.87	3.49	3.57	1.46	1.80	1.65	1.46	–	0.94	2.24	2.02	0.74
Er	5.51	10.20	10.30	4.58	5.50	4.97	4.58	–	2.81	6.48	6.01	2.25
Tm	0.83	1.69	1.71	0.68	0.83	0.74	0.68	–	0.43	0.93	0.86	0.33
Yb	5.04	10.00	10.10	4.50	5.42	4.94	4.50	–	2.97	6.38	5.55	2.29
Lu	0.78	1.52	1.48	0.69	0.85	0.77	0.69	–	0.48	1.03	0.86	0.31
Hf	9.68	17.00	15.50	6.53	9.21	9.89	6.53	–	4.33	5.02	6.80	2.96
Ta	1.40	2.32	1.91	0.79	1.45	1.38	0.79	–	2.49	1.75	1.00	1.60
W	1.38	2.16	2.24	0.50	0.64	0.50	0.50	–	0.17	0.26	0.64	0.72
Pb	27.00	29.50	16.80	6.67	21.85	9.53	6.67	–	6.54	21.86	7.16	16.23
Th	17.50	14.70	14.20	8.13	11.59	11.76	8.13	–	4.96	5.42	8.77	35.19
U	2.63	2.96	2.22	1.07	2.55	2.31	1.07	–	0.77	0.74	1.76	2.65
Ti	1175.83	849.81	932.51	2969.14	2157.48	1977.69	1726.23	483.93	2157.48	3116.36	1078.74	895.95
P	133.60	69.86	147.13	721.78	261.96	349.28	228.16	118.03	305.62	567.58	130.98	160.23
$(La/Yb)_n$	8.12	5.06	3.94	6.09	6.24	5.31	6.09	–	14.83	15.21	9.05	10.42
Eu/Eu*	0.08	0.04	0.08	0.48	0.58	0.34	0.48	–	0.25	0.26	0.04	0.40
Tzr	870	931	956	797	861	859	808	–	784	790	829	725

FeO* = 0.9 FeO + F_2O_3; ASI = (Al/(Ca–1.67 P + Na + K)); MALI = (Na_2O + K_2O–CaO); *T*°C is the temperature of saturation in Zr obtained using the thermometer, after [70].

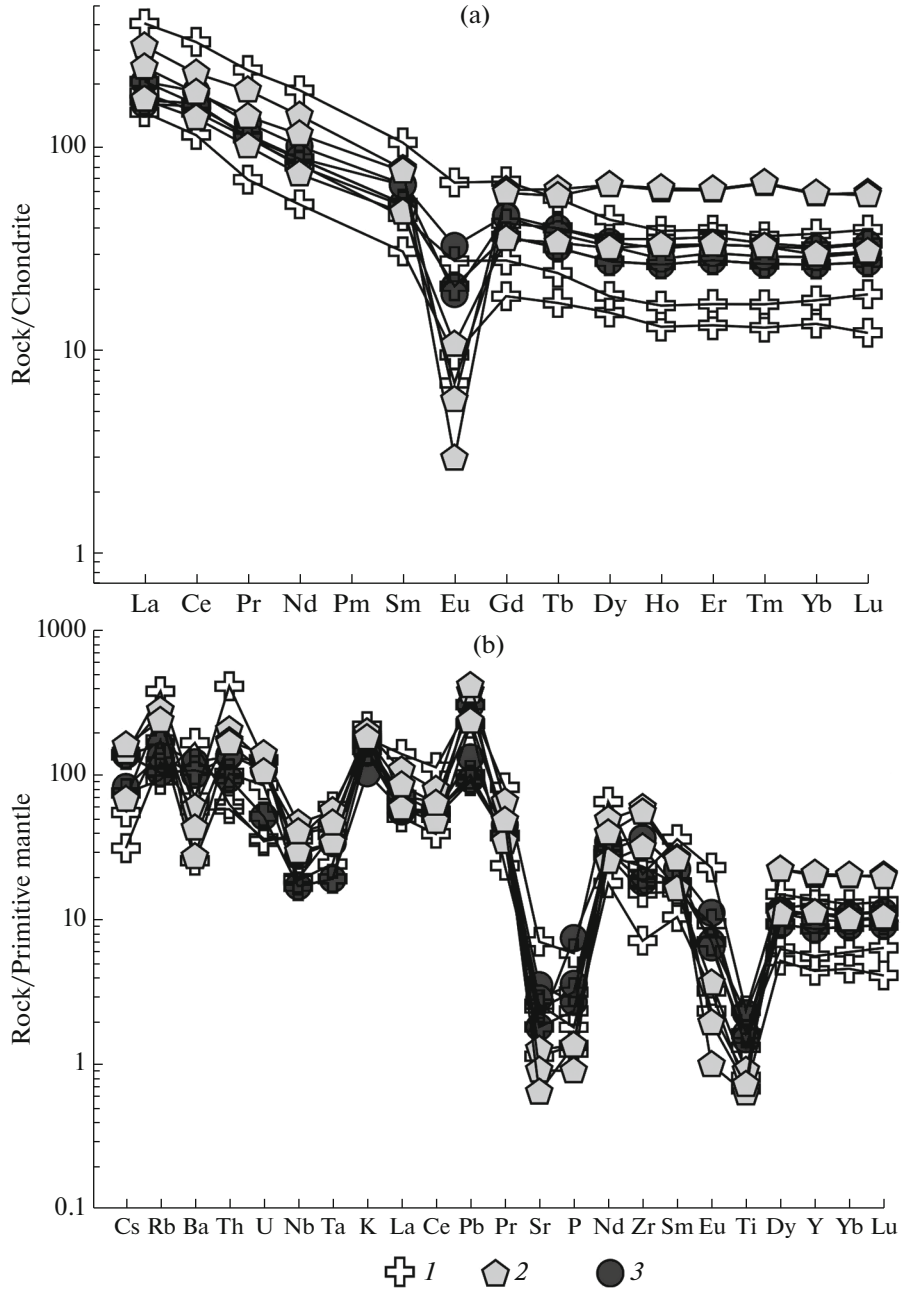

Fig. 13. The distribution of rare and rare-earth elements in the rocks of the Aktass association, after [61]. (a) Chondrite-normalized; (b) normalized to the composition of the primitive mantle. (*1*) Granite of the Aktass Complex; (*2*) effusive rocks of the Aktass Formation; (*3*) effusive rocks of the Kumola Formation.

area of melt generation, which most likely should have been reflected in both the chemical and mineral compositions of effusive rocks and granitoids of the Aktass association.

THE TECTONIC EVOLUTION OF THE SOUTHERN ULUTAU IN THE NEOPROTEROZOIC

The data we obtained and that available indicate the formation of the structural–material complexes of the pre-Vendian basement of the Southern Ulutau in the Tonian period of the Neoproterozoic. However, variations in age estimates and isotope–geochemical characteristics suggest a difference in the time and setting of the formation of the Tonian complexes in the western and eastern parts of the Ulutau Terrane (Fig. 15).

The reported isotope–geochemical characteristics of felsic igneous rocks of the Dyusembai and Aktass associations are characteristic of anorogenic-type igneous rocks. The wide occurrence of coarse-clastic rocks, including conglomerate with pebbles of felsic

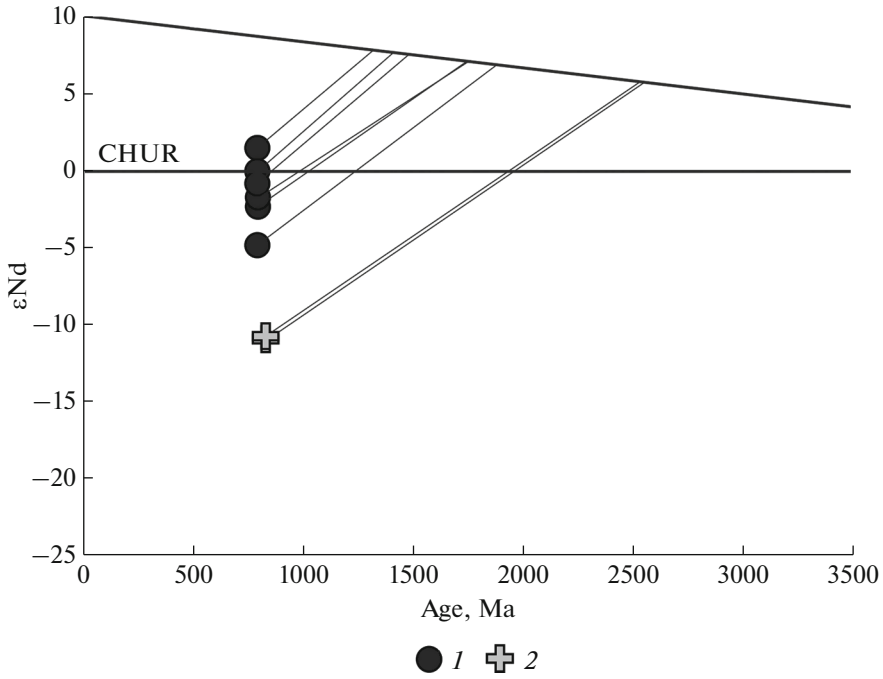

Fig. 14. The diagram of the evolution of the Nd isotope composition of igneous rocks of the Dyusembai and Aktass volcanic–plutonic associations. The line of the evolution of the depleted mantle is shown (oblique line) after [24]. CHUR, homogeneous chondrite reservoir, after [35]. (*1*) Rocks of the Aktass association; (*2*) rocks of the Dyusembai association.

volcanic rocks and granitoids, in the overlying volcanogenic–sedimentary sequences of the Maityubinsk and Bozdak groups indicates the riftogenic setting of the formation of the complexes (Fig. 3).

Based on this, the obtained age estimates (830 and 790–800 Ma) of the formation of two rhyolite–granite associations characterize the beginning of the stage of continental rifting.

There are no Precambrian rhyolite–granite associations within the eastern part of the Southern Ulutau, while the pre-Vendian basement complexes are represented by volcanic and basalt–andesite–rhyolitic tuff

Table 5. A summary of the results of the Sm–Nd isotope study of volcanic rocks and granitoids of the Dyusembai and Aktass associations

Sample	Rock	Age	Sm (ppm)	Nd (ppm)	$^{147}Sm/^{144}Nd$	$^{143}Nd/^{144}Nd$	$\varepsilon_{Nd}(T)$	$t_{Nd}DM$
U-9006	Granite of the Zhaunkar Complex	829	0.62	2.99	0.1253	0.511687 ± 4	−11.0	2513
U-9008	Granite of the Zhaunkar Complex	829	5.97	28.6	0.1259	0.511698 ± 5	−10.8	2510
TS-1177	Rhyolite of the Aktass Formation	794	9.52	46.1	0.1249	0.512139 ± 4	−2.4	1733
TS-1180	Rhyolite of the Aktass Formation	794	12.80	58.2	0.1331	0.512215 ± 4	−1.8	1765
TS-1175	Granite of the Aktass Complex	791	6.95	37.9	0.1110	0.512267 ± 5	1.4	1310
TS-1176	Granite of the Aktass Complex	791	15.37	79.1	0.1175	0.512224 ± 2	−0.1	1466
TS-1179	Granite of the Aktass Complex	791	9.18	46.9	0.1184	0.511983 ± 4	−4.9	1863
U-9002	Granite of the Aktass Complex	791	8.51	46.4	0.1108	0.512148 ± 5	−0.9	1483

$\varepsilon_{Nd}(T)$ values are calculated for an age of 800 Ma.

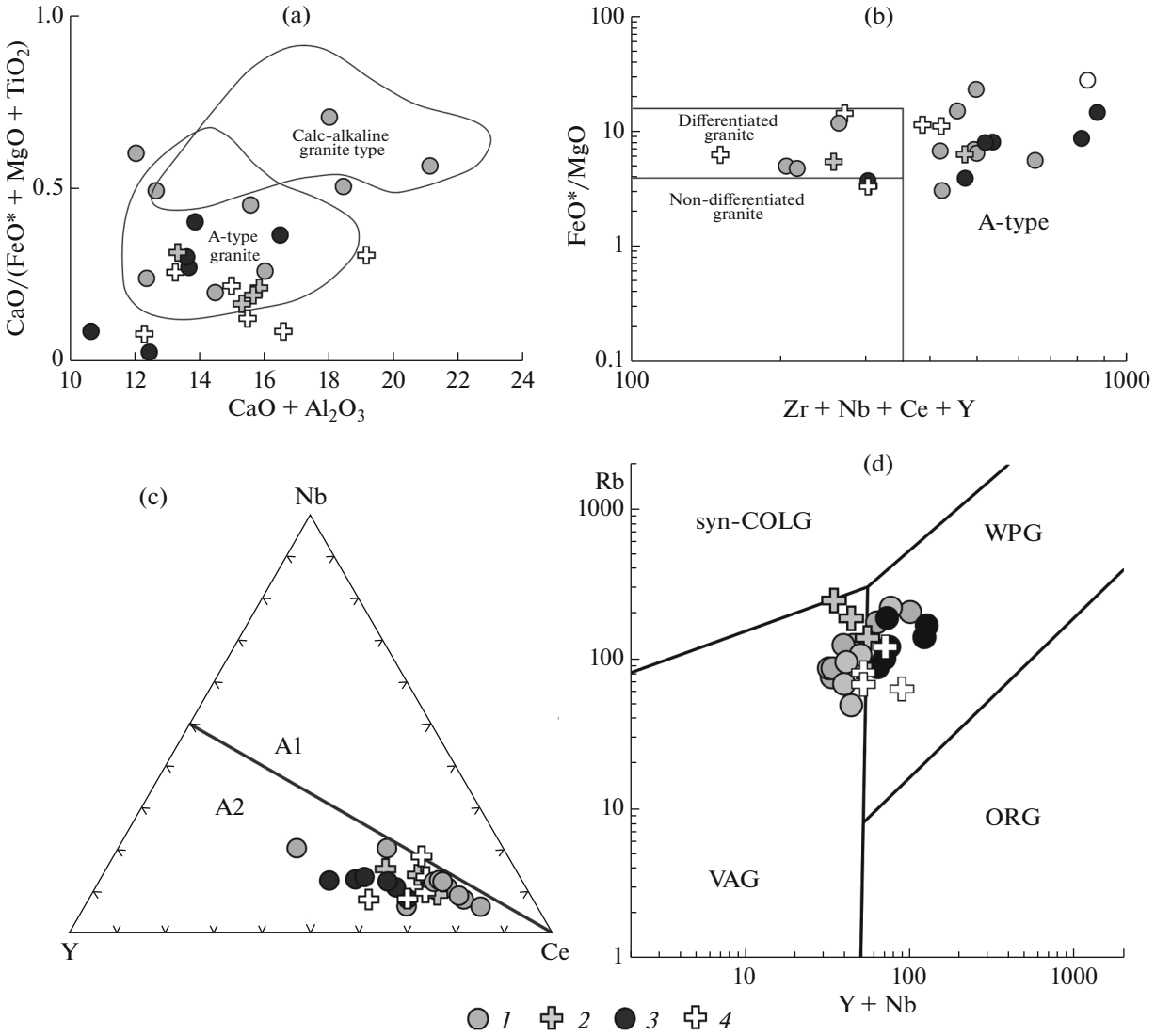

Fig. 15. Tectonomagmatic discrimination diagrams for the rocks of the Dyusembai and Aktass volcanic–plutonic associations. (a) $CaO/(FeO^* + MgO + TiO_2)$–$CaO + Al_2O_3$, after [22]; (b) FeO^*/MgO–Zr + Nb + Ce + Y, after [68]; (c) Y–Nb–Ce, after [24]; (d) Rb–Y + Nb, after [50]. (*1*) Effusive rocks of the Dyusembai and Zhaunkar formations; (*2*) granitoids of the Zhaunkar Complex; (*3*) effusive rocks of the Aktass and Kumolin formations; (*4*) granitoids of the Aktass Complex.

associated with terrigenous and chemogenic sedimentary rocks (Fig. 3).

The differentiated character of magmatism and other compositional patterns indicate the formation of parental melts for this complex in a suprasubduction setting [10]. The Nd isotope characteristics of felsic volcanic and tuffaceous rocks (εNd from –2.0 to –2.5; T(Nd)DM = 1.8–2.3 Ga) indicate the evolution of a suprasubduction system on the continental crust; the crustal complexes, including Early Precambrian ones, were involved in the formation of melts [11].

The differentiated volcanic sequences in the eastern part are younger than the rhyolite–granite associations in the western part of the terrane; their formation occurred in the second half of the Tonian, but in the interval from ~780 to ~740 Ma [10–12].

However, the predominance of a significant population of nonrounded crystals with age estimates from 900 to 1100 Ma and variations in εHf(t) from –15 to +8 in volcanic–sedimentary rocks among grains of detrital zircon suggests the onset of suprasubduction magmatism at the end of the Mesoproterozoic–beginning of the Neoproterozoic [11].

Thus, the Tonian magmatism in the western part of the terrane was associated with the processes of continental rifting, while that in the eastern part of the terrane was associated with subduction processes. The onset of suprasubduction processes at the end of the Mesoproterozoic–beginning of the Neoproterozoic allows us to consider the tectonic–magmatic evolution of the Southern Ulutau in the Tonian period in the regime of an active continental margin.

The differentiated volcanic series in its eastern part (modern coordinates) were formed due to suprasubduction magmatism caused by subduction of the oceanic lithosphere.

The formation of two rhyolite–granite associations in the western part of the Southern Ulutau occurred in a rifting setting caused by their rearward location relative to the subduction front.

COMPARISON OF THE STRUCTURE OF NEOPROTEROZOIC COMPLEXES OF THE SOUTHERN ULUTAU WITH TERRANES OF THE ULUTAU–MOYUNKUM GROUP

The Neoproterozoic felsic igneous complexes are a characteristic structural element of the Precambrian terranes of the Ulutau–Moyunkum group [23].

They are represented by orthogneiss (800 ± 9 Ma), metarhyolite of the Kopin Formation (794 ± 5 Ma) of the Kendyktas Block, and orthogneiss (789 ± 5 Ma) of the Chuya and Atyuz (799–840 Ma) blocks within the Chuya–Kendyktas Terrane [37, 59, 63]. In the Zheltav Terrane, these complexes include felsic volcanic rocks (829 ± 5 Ma) and orthogneiss (780–790 Ma) [51, 60].

The complexes of this type in the Karatau–Talas Terrane include tuff of the Kurgan Formation (780–760 Ma) [7, 39, 45]. In the Karatau–Dzhebagly Terrane, such complexes are represented by the basalt–rhyolite Kainar Formation and granitoids of the Kumyst Complex (717 ± 4 Ma) [2, 3].

The Neoproterozoic igneous complexes in the Middle Tien Shan Terrane are represented by granitoids of the Beshtor (893 ± 3 Ma) and Sarydzhaz (831 ± 8 Ma) complexes, as well as felsic volcanic rocks of the Bolshoi Naryn Formation (840–720 Ma) [31, 56, 62].

The isotope–geochemical characteristics of the Neoproterozoic felsic volcanic rocks and granitoids of the Precambrian terranes of Southwest Kazakhstan and the Middle Tien Shan allow us to classify them as A-2-type granite and to accept the complexes of the Early Precambrian continental crust as the major melt source [23, 37, 51, 63]. Similar age estimates suggest that in the Neoproterozoic, mainly in the Tonian time, the Precambrian terranes of the Ulutau-Moyunkum group were part of a single continental marginal igneous belt, in the rear part of which rifting processes were accompanied by the formation of thick units of felsic volcanic rocks and granitoids.

The features of the structure, composition, and age of the Precambrian complexes make possible to consider the terranes of the Ulutau–Moyunkum group as formations related to the Tarim Craton [23] (Fig. 16).

Its structure includes, among others, the Early Precambrian complexes (Heluositan and Tuogelakebudake), which were the major sources of melts and clastic material for the Proterozoic igneous formations and terrigenous sequences [79].

The tectonomagmatic evolution of the craton in the Neoproterozoic (Tonian period) included the development of its northern part in the active marginal regime [52, 53, 75, 76, 78]. At the same time, the Neoproterozoic evolution of both northern and southern margins of the Tarim Craton included riftogenic events, while they differed in ages and compositional patterns of igneous rocks (Fig. 16).

The continental rifting on the southern margin of the Tarim Craton was accompanied by the formation of granitoids (Kalakashi Group) and bimodal volcanogenic series (Salaidzhiazitazh Group) with ages of ~900–850 Ma, mafic and basaltic dykes (~800 Ma) [66, 76, 77, 80]. These rifting events coincide with the main stage of suprasubduction magmatism on the northern margin of the Tarim (Aksu, Kuruktag), which included the formation of andesite (908–903 Ma) [33], granitoids, including those with adakitic characteristics (830–785 Ma) [30, 41], mafic–ultramafic intrusions, and dyke swarms in the interval of 820–760 Ma [74].

The reverse migration of the subduction system to the south began at the northern margin at the end of the Tonian period [53]. These events included the beginning of rifting processes in the back-arc region, which was first recorded by mafic dykes with ages of 773–759 Ma [73] and subsequently led to the formation of a back-arc basin with characteristic bimodal volcanism (740–725 Ma) [53, 71], which proceeded until the Ediacaran.

The close age of the formation and composition of the Neoproterozoic igneous complexes suggest that the Precambrian terranes of the Ulutau–Moyunkum Group and the Tarim Craton are the fragments of a large igneous belt, which was confined to the active NW margin of the Rodinia Supercontinent [30, 78] (Fig. 17).

The long-term subduction of the oceanic lithosphere of the Panrodinian Ocean along the periphery of the supercontinent, which began as early as the end of the Mesoproterozoic, led to the rise of the mantle plume in the rear parts, which contributed to the onset

Fig. 16. The correlation scheme for the structural–material complexes of the Southern Ulutau and Tarim Craton, compiled after [30, 33, 41, 53, 58, 66, 67, 70, 72–81]. (*1*) Sandstone; (*2*) limestone; (*3*) quartz–feldspar shale; (*4*) phyllite; (*5*) tillite and coarse clastic tillite-like conglomerate; (*6*) boulder and large-pebble conglomerate; (*7*) quartz shale; (*8*) monomineral and muscovite quartzite; (*9*) ferruginous quartzite; (*10*) basic tuff conglomerate; (*11*) basalt; (*12*) andesite; (*13*) tuff of the intermediate composition; (*14*) rhyolite and rhyodacite; (*15*) felsic tuff; (*16*) shale and gneisse; (*17*) syenite; (*18*) carbonatite; (*19*) gabbro and ultramafic rocks; (*20*) granitoids; (*21*) dykes of the basic composition.

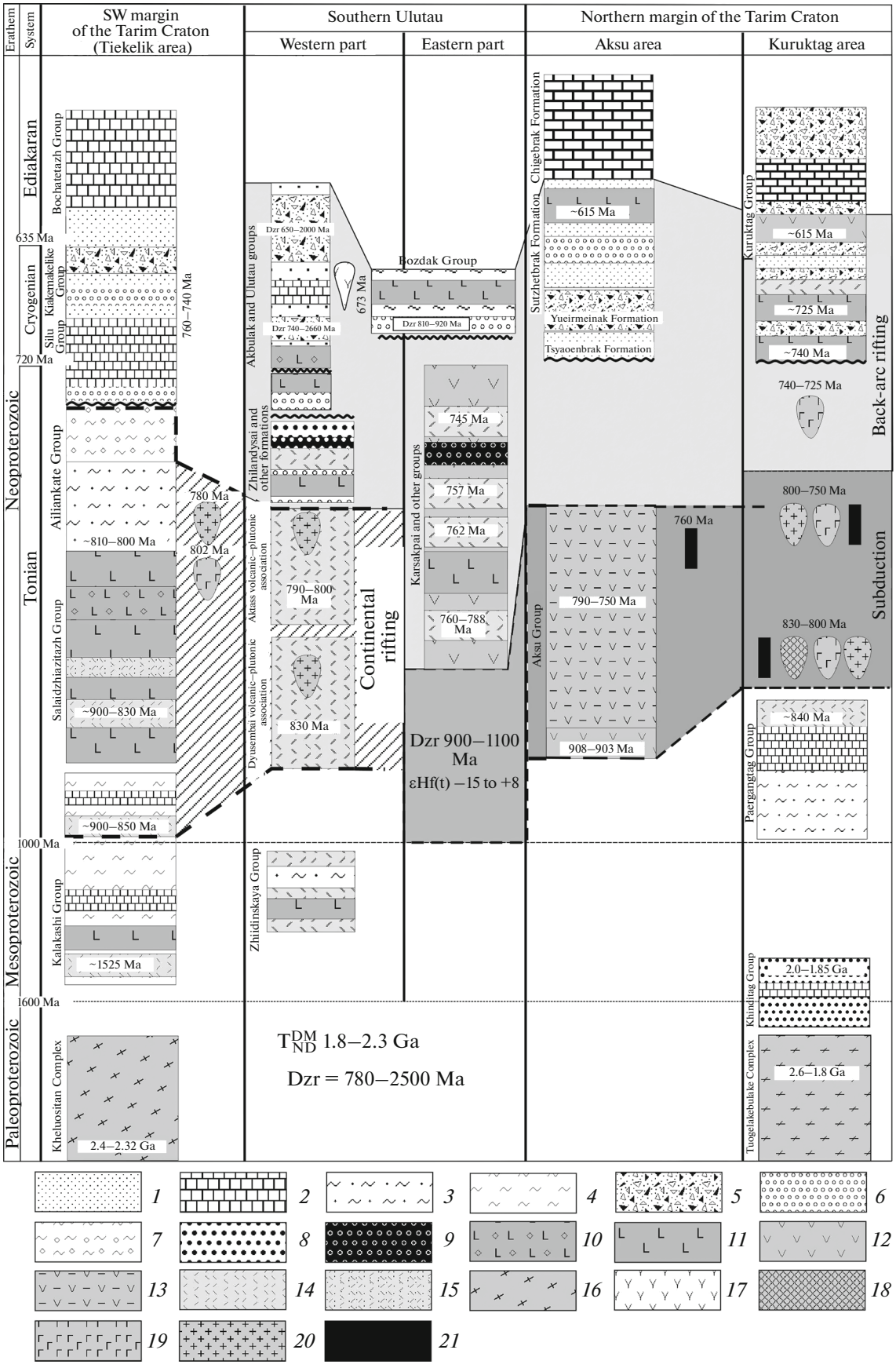
Erathem
System
SW margin of the Tarim Craton (Tiekelik area)
Southern Ulutau
Western part
Eastern part
Northern margin of the Tarim Craton
Aksu area
Kuruktag area
Neoproterozoic
Mesoproterozoic
Paleoproterozoic
Ediakaran
Cryogenian
Tonian
635 Ma
720 Ma
1000 Ma
1600 Ma
Bochatetazh Group
Kiakemakelike Group
Silu Group
760–740 Ma
Ailiankate Group
~810–800 Ma
780 Ma
802 Ma
Salaidzhiazitazh Group
~900–830 Ma
~900–850 Ma
Kalakashi Group
~1525 Ma
Kheluositan Complex
2.4–2.32 Ga
Akbulak and Ulutau groups
Dzr 650–2000 Ma
673 Ma
Dzr 740–2660 Ma
Bozdak Group
Dzr 810–920 Ma
Zhilandysai and other formations
Aktass volcanic–plutonic association
790–800 Ma
Dyusembai volcanic–plutonic association
830 Ma
Zhiidinskaya Group
Karsakpai and other groups
745 Ma
757 Ma
762 Ma
760–788 Ma
Continental rifting
Dzr 900–1100 Ma
εHf(t) –15 to +8
T^{DM}_{ND} 1.8–2.3 Ga
Dzr = 780–2500 Ma
Chigebrak Formation
~615 Ma
Sutzhetbrak Formation
Yueirmeinak Formation
Tsyaoenbrak Formation
760 Ma
Aksu Group
790–750 Ma
908–903 Ma
Kuruktag Group
~615 Ma
~725 Ma
~740 Ma
740–725 Ma
Back-arc rifting
800–750 Ma
830–800 Ma
Subduction
~840 Ma
Paergangtag Group
Khinditag Group
2.0–1.85 Ga
Tuogelakebulake Complex
2.6–1.8 Ga
1
2
3
4
5
6
7
8
9
10
11
12
13
14
15
16
17
18
19
20
21

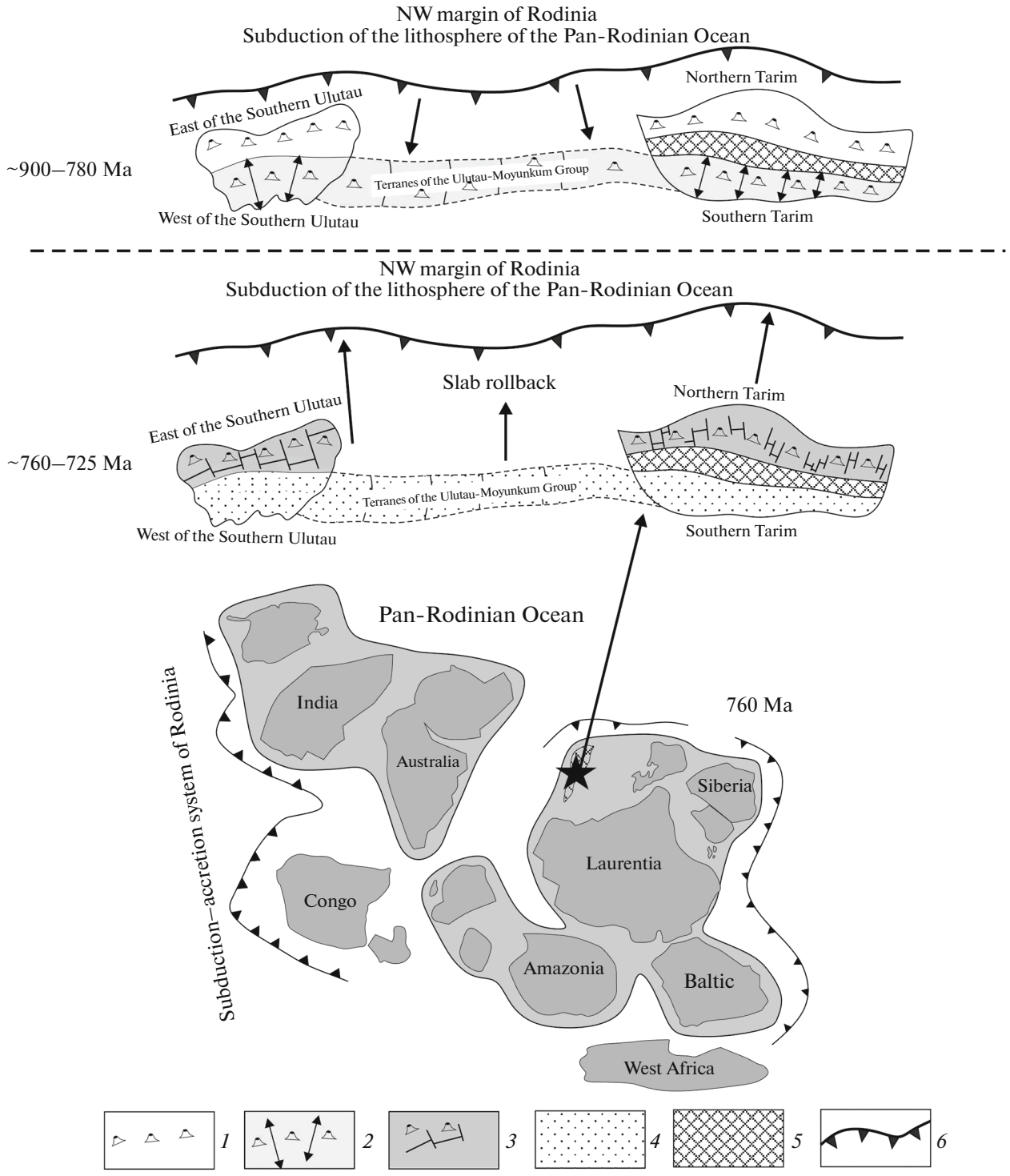

Fig. 17. Southern Ulutau and Tarim Craton in the Neoproterozoic. (a) Paleogeographic position, after [27, 30]; (b) scheme of the tectonic evolution. (*1*–*3*) Area of magmatism: (*1*) island-arc, (*2*) rear riftogenic, (*3*) back-arc riftogenic; (*4*) area of the passive continental margin; (*5*) Central Tarim; (*6*) direction of subduction.

of rifting and initiated the breakup of the Rodinia Supercontinent [17, 40].

At the same time, the formation of rhyolite–granite associations both in the western part of the Southern Ulutau and on the other terranes of the Ulutau–Moyunkum Group coincided with the stage of Tonian within-plate magmatism at the southern margin of the Tarim Craton (Fig. 16).

Differentiated basalt–andesite–rhyolite magmatism in the eastern part of the Southern Ulutau (~780–740 Ma) coincided with the beginning of back-arc rifting at the northern margin of the craton (773–759 Ma) [10–12, 73] (Fig. 16).

CONCLUSIONS

(1) Our new data on the structure, composition, and ages of the Neoproterozoic complexes in the western part of the Southern Ulutau allowed us to identify two rhyolite–granite volcanic–plutonic associations in the structure of this block: Dyusembai and Aktass, with ages of ~830 and ~790 Ma, respectively.

(2) Felsic volcanic rocks and their comagmatic granitoids have geochemical characteristics of an anarogenic type and their parental melts were formed under intraplate conditions and with the participation of complexes of the Early Precambrian continental crust.

(3) The tectonomagmatic evolution of the Southern Ulutau in the Neoproterozoic occurred in the setting of an active continental margin. The complexes of the eastern part of the Southern Ulutau were formed within an ensialic island arc, while the complexes of the western part of the Southern Ulutau were formed in the area of rift magmatism in the rear region.

(4) Tonian magmatism in the Southern Ulutau, as well as in other terranes of the Ulutau–Moyunkum group, was due to their inclusion in the basement of a large volcanic–plutonic belt, which marked the processes of subduction of the oceanic lithosphere beneath the NW margin of the Rodinia Supercontinent.

ACKNOWLEDGMENTS

The authors thank the reviewers, Academician V.V. Yarmolyuk (Institute of Geology of Ore Deposits, Petrography, Mineralogy, and Geochemistry, Russian Academy of Sciences, Moscow, Russia), Dr. T.V. Donskaya (Institute of the Earth's Crust, Siberian Branch, Russian Academy of Sciences, Irkutsk, Russia) for comments that allowed us to improve the manuscript, and the editor M.N. Shoupletsova (Geological Institute, Russian Academy of Sciences, Moscow, Russia) for thorough editing.

FUNDING

The study was supported by the Russian Science Foundation, project no. 22-17-00069, and was performed as a part of the State Task of the Geological Institute, Russian Academy of Sciences. Analytical study was supported by the Russian Foundation for Basic Research, project no. 20-05-00108.

CONFLICT OF INTEREST

The authors declare that they have no conflicts of interest.

REFERENCES

1. D. V. Alekseev, K. E. Degtyarev, A. A. Tretyakov, and N. A. Kanygina, "Early Neoproterozoic (~920 Ma) granite–gneiss of the Junggar Alataw, South Kazakhstan: Age substantiation based on the results of U–Th–Pb (SIMS) dating," Dokl. Earth Sci. **496** (1), 13–16 (2021).
2. *Geology and Metallogeny of the Karatau. Vol. 1. Geology*, Ed. by I. F. Nikitin (Nauka, Alma-ata, 1986) [in Russian].
3. K. E. Degtyarev, A. A. Tretyakov, E. B. Sal'nikova, and A. B. Kotov, "The Late Cryogenian age of the Kumysty granosyenite complex, Greater Karatau, Southern Kazakhstan," Dokl. Earth Sci. **484** (2), 120–123 (2019).
4. N. V. Dmitrieva, E. F. Letnikova, and A. I. Proshenkin, "The formation time of the Zhiida Group of the Maityube Zone (Southern Ulutau, Central Kazakhstan)," in *Proceedings of VI Russian Conference on Isotope Geochronology "Isotope Dating of Geological Processes: New Results, Approaches and Perspectives," June 2–5, 2015, IPGG RAS, St. Petersburg*) (Sprnter, St. Petersburg, 2015), pp. 76–77.
5. P. V. Ermolov, *Actual Problems in Isotope Geology and Metallogeny of Kazakhstan* (KPU, Karaganda, 2013 [in Russian].
6. V. S. Mileev and S. B. Rozanov, *Precambrian Geology and Tectonics of Central Kazakhstan*, Ed. by Yu. A. Zaitsev (Mosk. Gos. Univ., Moscow, 1976) [in Russian].
7. Yu. K. Sovetov, "Neoproterozoic rifting and evolution of sedimentary basins on the Tarim-type microcontinents: Lesser Karatau, Southern Kazakhstan," in *Proceedings of V All-Russian Lithological Conference "Types of Sedimentogenesis and Lithogenesis in the Earth's History," October 14–16, 2008, IGG UBr RAS, Ekaterinburg* (Inst. Geol. Geokhim. Ural. Otd. Ross. Akad.Nauk, Ekaterinburg, 2008), pp. 287–289.
8. *Types of Magmas and their Sources in the Earth's History. Part 1. Magmatism and Geodynamics—Main Factors of the Earth's Evolution*, Ed. by O. A. Bogatikov and V. I. Kovalenko (IGEM Ross. Akad. Nauk, Moscow, 2006) [in Russian].
9. A. A. Tretyakov, K. E. Degtyarev, E. B. Sal'nikova, K. N. Shatagin, A. B. Kotov, I. V. Anisimova, and Yu. V. Plotkina, "The late Tonian Zhaunkar granite complex of the Ulutau sialic massif, Central Kazakhstan," Dokl. Earth Sci. **473** (2), 411–415 (2017).
10. A. A. Tretyakov, K. E. Degtyarev, N. A. Kanygina, and N. K. Danukalov, "The Late Neoproterozoic age of differentiated volcanic complexes of the Ulutau Massif: Results of U–Th–Pb (SIMS) dating," Dokl. Earth Sci. **494** (1), 670–674 (2020).
11. A. A. Tretyakov, K. E. Degtyarev, N. A. Kanygina, E. F. Letnikova, F. I. Zhimulev, V. P. Kovach, N. K. Danukalov, and H.-Y. Lee, "Late Precambrian metamorphic complexes of the Ulutau Massif (Central Kazakhstan): Age, composition, and formation settings of protoliths," Geotectonics **54** (5), 605–627 (2020).
12. A. A. Tretyakov, K. E. Degtyarev, N. K. Danukalov, and N. A. Kanygina, "Neoproterozoic age of the iron ore volcanogenic-sedimentary series of the Ulutau Terrane (Central Kazakhstan)," Dokl. Earth Sci. **502** (2), 1–6 (2022).

13. L. I. Filatova, *Stratigraphy and Historical-Geological (Formational) Analysis of Metamorphic Formations of the Precambrian of Central Kazakhstan* (Nedra, Moscow, 1983) [in Russian].
14. L. I. Filatova and N. A. Bogatyreva, "On the most ancient Precambrian deposits of the Southern Ulutau," in *Proceedings of Conference on Geology of Central Kazakhstan "Problems of Geology of Central Kazakhstan*," Ed. by A. A. Bogdanov (Mosk. Gos. Univ., Moscow, 1971), vol. 10, pp. 92–106) [in Russian].
15. V. V. Yarmolyuk and V. I. Kovalenko, *Rift Magmatism of Active Continental Margins and its Ore Potential* (Nauka, Moscow, 1991) [in Russian].
16. B. Bonin, "A-type granites and related rocks: Evolution of a concept, problems and prospects," Lithos **97**, 1–29 (2007).
17. P. A. Cawood, R. A. Strachan, S. A. Pisarevsky, D. P. Gladkochub, and J. B. Murphy, "Linking collisional and accretionary orogens during Rodinia assembly and breakup: Implications for models of supercontinent cycles," Earth Planet. Sci. Lett. **449**, 118–126 (2016).
18. J. Chorowicz, "The East African Rift System," J. Afr. Earth Sci. **43**, 379–410 (2005).
19. J. D. Clemens, J. R. Holloway, and A. J. R. White, "Origin of an A-type granite: Experimental constraints," Am. Mineralogist **71**, 317–324 (1986).
20. B. J. Collins, S. D. Beams, A. J. R. White, and B. W. Chappel, "Nature and origin of A-type granites with particular reference to southeastern Australia," Contrib. Mineral. Petrol. **80**, 189–200 (1982).
21. R. A. Creaser and R. C. Price, "A-type granites revisited: Assessment of a residual-source model," Geology **19**, 163–166 (1991).
22. R. Dall'Agnol and D. C. Oliveira, "Oxidized, magnetite-series, rapakivi-type granites of Carajás, Brazil: Implications for classification and petrogenesis of A-type granites," Lithos **93**, 215–233 (2007).
23. K. Degtyarev, A. Yakubchuk, A. Tretyakov, A. Kotov, and V. Kovach, "Precambrian geology of the Kazakh Uplands and Tien Shan: An overview," Gondwana Res. **47**, 44–75 (2017).
24. D. J. Depaolo, "Neodymium isotopes in the Colorado Front Range and crust-mantle evolution in the Proterozoic," Nature **291**, 193–196 (1981).
25. G. N. Eby, "The A-type granitoids—a review of their occurrence and chemical characteristics and speculations on their petrogenesis," Lithos **26**, 115–134 (1990).
26. G. N. Eby, "Chemical subdivision of the A-type granitoids-petrogenetic andtectonic implications," Geology **20**, 641–644 (1992).
27. D. Evans, "Meso-Neoproterozoic Rodinia supercycle," in *Ancient Supercontinents and the Paleogeography of Earth*, Ed. by L. Pesonen, J. Salminen, S.-A. Elming, D. Evans, and T. Veikkolainen (Elsevier, NY, USA. 2022), pp. 549–568.
28. B. R. Frost, C. G. Barnes, W. J. Collins, R. J. Arculus, D. J. Ellis, and C. D. Frost, "A geochemical classification for granitic rocks," J. Petrol. **42**, 2033–2048 (2001).
29. C. D. Frost and B. R. Frost, "On ferroan (A-type) granitoids: Their compositional variability and modes of origin," J. Petrol. **52**, 39–53 (2010).
30. R. Ge, W. Zhu, S. A. Wilde, J. He, X. Cui, X. Wang, and Z. Bihai, "Neoproterozoic to Paleozoic long-lived accretionary orogeny in the northern Tarim Craton," Tectonics **33**, 302–329 (2014).
31. S. Glorie, J. De Grave, M. M. Buslov, F. I. Zhimulev, D. F. Stockli, V. Y. Batalev, A. Izmer, P. Van den Haute, F. Vanhaecke, and M. A. Elburg, Tectonic history of the Kyrgyz South Tianshan (Atbashi–Inylchek) suture zone: The role of inherited structures during deformation-Propagation, Tectonics **30** (6), p. TC6016 (2011).
32. S. J. Goldstein and S. B. Jacobsen, "Nd and Sr isotopic systematics of river water suspended material implications for crystal evolution," Earth Planet. Sci. Lett. **87**, 249–265 (1988).
33. J. Y. He, B. Xu, and D. Li, "Newly discovered early Neoproterozoic (ca. 900 Ma) andesitic rocks in the northwestern Tarim Craton: Implications for the reconstruction of the Rodinia supercontinent," Precambrian Res. **325**, 55–68 (2019).
34. A. Q. Hu, G. J. Wei, B. M. Jahn, J. B. Zhang, W. F. Deng, and L. L. Chen, "Formation of the 0.9 Ga Neoproterozoic granitoids in the Tianshan Orogen, NW China: Constraints from the SHRIMP zircon age determination and its tectonic significance," Geochimica **9**, 197–212 (2010) [in Chinese with English abstr.].
35. S. B. Jacobsen and G. J. Wasserburg, "Sm–Nd evolution of chondrites and achondrites," Earth Planet. Sci. Lett. **67**, 137–150 (1984).
36. B. M. Jahn, F. Y. Wu, and B. Chen, "Massive granitoid generation in Central Asia: Nd isotopic evidence and implication for continental growth in the Phanerozoic," Episodes **43**, 82–92 (2000).
37. A. Kröner, D. V. Alexeiev, E. Hegner, Y. Rojas-Agramonte, M. Corsini, Y. Chao, J. Wong, B. F. Windley, D. Liu, and A. A. Tretyakov, "Zircon and muscovite ages, geochemistry and Nd–Hf isotopes for the Aktyuz metamorphic terrane: evidence for an Early Ordovician collision belt in the northern Tianshan of Kyrgyzstan," Gondwana Res. **21**, 901–927 (2012).
38. M. J. Le Bas, R. W. Le Maitre, A. Streckeisen, and B. Zanettin, "A chemical classification of volcanic rocks based on the total alkali-silica diagram," J. Petrol. **27**, 745–750 (1986).
39. N. M. Levashova, J. G. Meert, A. S. Gibsher, W. C. Grice, and M. L. Bazhenov, "The origin of microcontinents in the Central Asian Orogenic Belt: Constraints from paleomagnetism and geochronology," Precambrian Res. **185**, 37–54 (2011).
40. Z. X. Li, S. V. Bogdanova, A. S. Collins, A. Davidson, B. de Waele, R. E. Ernst, I. C. W. Fitzsimons, R. A. Fuck, D. P. Gladkochub, J. Jacobs, K. E. Karlstrom, S. Lu, L. M. Natapov, V. Pease, S. A. Pisarevsky, K. Thrane, and V. Vernikovsky, "Assembly, configuration, and break-up history of Rodinia: a synthesis," Precambrian Res. **160**, 179–210 (2008).
41. X.-P. Long, C. Yuan, M. Sun, A. Kröner, G.-C. Zhao, S. Wilde, and A.-Q. Hu, Reworking of the Tarim Craton by underplating of mantle plume-derived magmas: Evidence from Neoproterozoic granitoids in the Kuluketage area, NW China," Precambrian Res. **187**, 1–14 (2011).

42. K. R. Ludwig, *ISOPLOT 3.00. A User's Manual* (Berkeley Geochron. Center Spec. Publ., 2003, No. 4).

43. K. R. Ludwig, *SQUID 1.00. A User's Manual* (Berkeley Geochron. Center Spec. Publ., 2000, No. 2).

44. R. Macdonald, "Nomenclature and petrochemistry of the peralkaline oversaturated extrusive rocks," Bull. Volcanol. **38**, 498–516 (1974).

45. J. G. Meert, A. S. Gibsher, N. M. Levashova, W. C. Grice, G. D. Kamenov, and A. B. Ryabinin, "Glaciation and ~770 Ma Ediacaran (?) fossils from the lesser Karatau microcontinent, Kazakhstan," Gondwana Res. **19**, 867–880 (2011).

46. A. S. Merdith, A. S. Collins, S. E. Williams, S. Pisarevsky, J. D. Foden, D. B. Archibald, M. L. Blades, B. L. Alessio, S. Armistead, D. Plavsa, C. Clark, and R. D. Müller, "A full-plate global reconstruction of the Neoproterozoic," Gondwana Res. **50**, 84–134 (2017).

47. C. F. Miller, S. M. McDowell, and R. W. Mapes, "Hot and cold granites? Implications of zircon saturation temperatures and preservation of inheritance," Geology **31**, 529–532 (2003).

48. R. D. Nance, J. B. Murphy, and M. Santosh, "The supercontinent cycle: A retrospective essay," Gondwana Res. **25**, 4–29 (2014).

49. A. E. Patiño Douce, "Generation of metaluminous A-type granites by lower pressure melting of calc-alkaline granitoids," Geology **25**, 743–746 (1997).

50. J. A. Pearce, N. W. Harris, and A. G. Tindle, "Trace element discrimination diagrams for the tectonic interpretation of granitic rocks," J. Petrol. **25**, 956–983 (1984).

51. A. V. Pilitsyna, A. A. Tretyakov, K. E. Degtyarev, E. B. Salnikova, A. B. Kotov, V. P. Kovach, K.-L. Wang, and V. G. Batanova, "Early Palaeozoic metamorphism of Precambrian crust in the Zheltau terrane (Southern Kazakhstan, Central Asian Orogenic belt): *P–T* paths, protoliths, zircon dating and tectonic implications," Lithos **324–325**, 115–140 (2019).

52. *Precambrian Geology of China*, Ed. by M. Zhai (Springer, NY, USA, 2015).

53. R. Ren, S. W. Guan, S. C. Zhang, L. Wu, and H. Y. Zhang, "How did the peripheral subduction drive the Rodinia breakup: Constraints from the Neoproterozoic tectonic process in the northern Tarim Craton," Precambrian Res. **339**, 1–17 (2020).

54. J. J. W. Rogers and M. Santosh, "Configuration of Columbia, Mesoproterozoic supercontinent," Gondwana Res. **5**, 5–22 (2002).

55. V. A. Ramos, "Anatomy and global context of the Andes: Main geologic features and the Andean orogenic cycle," in *Backbone of the Americas: Shallow Subduction, Plateau Uplift, and Ridge and Terrane Collision,* Ed. by S. M. Kay, V. A. Ramos, and W. R. Dickinson, (GSA Mem., 2009, Vol. 204), pp. 31–65.

56. Y. Rojas-Agramonte, A. Kroner, D. V. Alexeiev, T. Jeffreys, A. K. Khudoley, J. Wong, H. Geng, L. Shug, S. A. Semiletkin, A. V. Mikolaichuk, V. V. Kiselev, J. Yang, and R. Seltmann, "Detrital and igneous zircon ages for supracrustal rocks of the Kyrgyz Tianshan and palaeogeographic implications," Gondwana Res. **26**, 957–974 (2014).

57. T. O. Rooney, "The Cenozoic magmatism of East Africa. Part V: Magma sources and processes in the East African Rift," Lithos **360–361**, 105296 (2020).

58. L.-S. Shu, X. L. Deng, W.-B. Zhu, D.-S. Ma, and W.-J. Xiao, "Precambrian tectonic evolution of the Tarim Block, NW China: New geochronological insights from the Quruqtagh domain," Precambrian Res. **42**, 774–790 (2011).

59. K. P. Skjerlie and A. D. Johnston, "Fluid-absent melting behaviour of a F-rich tonalitic gneiss at mid-crustal pressures: implications for the generation of anorogenic granites," J. Petrol. **34**, 785–815 (1993).

60. A. V. Skoblenko (Pilitsyna), K. E. Degtyarev, N. A. Kanygina, A. A. Tretyakov, S. Yu. Skuzovatov, K.-N. Pang, and H.-Y. Lee, "Precambrian and Early Palaeozoic metamorphic complexes in the SW part of the Central Asian Orogenic Belt: Ages, compositions, regional correlations and tectonic affinities," Gondwana Res. **105**, 117–142 (2022).

61. S. S. Sun and W. F. McDonough, "Chemical and isotopic systematic of oceanic basalts: Implications for mantle composition and processes," in *Magmatism in the Ocean Basins*, Ed. by A. D. Saunders and M. J. Norry (Spec. Publ.—Geol. Soc. London, 1989, Vol. 42), pp. 313–345.

62. B. Terbishalieva, M. J. Timmerman, A. Mikolaichuk, U. Altenberger, J. Sláma, A. M. Schleicher, M. Sudo, E. R. Sobel, and S. B. Cichy, "Calc-alkaline volcanic rocks and zircon ages of the late Tonian: early Cryogenian arc-related Big Naryn Complex in the Eastern Djetim-Too Range, Middle Tianshan block, Kyrgyzstan," Int. J. Earth Sci. **110**, 353–375 (2021).

63. A. A. Tretyakov, A. V. Pilitsyna, K. E. Degtyarev, N. A. Kanygina, E. B. Salnikova, V. P. Kovach, H.-Y. Lee, K.-L. Wang, V. G. Batanova, and E. V. Kovalchuk, "Neoproterozoic granitoid magmatism and granulite metamorphism in the Chu-Kendyktas terrane (Southern Kazakhstan, Central Asian orogenic belt): Zircon dating, Nd isotopy and tectono-magmatic evolution," Precambrian Res. **332**, p. 105397 (2019).

64. S. P. Turner, J. D. Foden, and R. S. Morrison, "Derivation of A-type magmas by fractionation of basaltic magma: An example from the Padthaway Ridge, South Australia," Lithos **28**, 151–179 (1992).

65. D. Vielzeuf and J. M. Montel, "Partial melting of metagreywackes. Part I. Fluid-absent experiments and phase relationship," Contrib. Mineral. Petrol. **117**, 375–393 (1994).

66. C. Wang, J. H. Zhang, M. Li, R. S. Li, and Y. Peng, "Generation of ca. 900–870Ma bimodal rifting volcanism along the southwestern margin of the Tarim Craton and its implications for the Tarim–North China connection in the Early Neoproterozoic," J. Asian Earth Sci. **113**, 610–625 (2015).

67. B. Wang, H. Liu, L. Shu, B. -M. Jahn, S. Chung, Y. Zha, and D. Liu, "Early Neoproterozoic crustal evolution in Northern Yili Block: insights from migmatite, orthogneiss and leucogranite of the Wenquan metamorphic complex in the NW Chinese Tianshan," Precambrian Res. **242**, 58–81 (2014).

68. J. B. Whalen, K. L. Currie, and B. W. Chappell, "A-type granites-geochemical char-acteristics, discrimination

and petrogenesis," Contrib. Mineral. Petrol. **95**, 407–419 (1987).

69. E. B. Watson and T. M. Harrison, "Zircon saturation revisited: Temperature and composition effects in a variety of crustal magma types," Earth Planet. Sci. Lett. **64**, 295–304 (1983).
70. I. S. Whilliams, "U–Th–Pb Geochronology by ion microprobe," Rev. Econom. Geol. **7**, 1–35 (1998).
71. B. Xu, P. Jian, H. Zheng, H. Zou, L. Zhang, and D. Liu, "U–Pb zircon geochronology and geochemistry of Neoproterozoic volcanic rocks in the Tarim Block of northwest China: Implications for the breakup of Rodinia supercontinent and Neoproterozoic glaciations," Precambrian Res. **136**, 107–123 (2005).
72. C.-L. Zhang, X.-H. Li, Z.-X. Li, S.-N. Lu, H.-M. Ye, and H.-M. Li, "Neoproterozoic ultramafic-carbonatite complex, granitoids in Quruqtagh of northeastern Tarim Block, western China: Geochronology, geochemistry and tectonic implications," Precambrian Res. **152**, 149–169 (2007).
73. C.-L. Zhang, Z.-X. Li, X.-H. Li, and H.-M. Ye, "Neoproterozoic mafic dyke swarms at the northern margin of the Tarim Block, NW China: Age, geochemistry, petrogenesis and tectonic implications," J. Asian Earth Sci. **35**, 167–179.
74. C. L. Zhang, H. B. Zou, H. K. Li, and H. Y. Wang, "Multiple phases of Neoproterozoic ultramafic-mafic complex in Kuruqtagh, northern margin of Tarim: Interaction between plate subduction and mantle plume?" Precambrian Res. **222–223**, 488–502 (2012).
75. C.-L. Zhang, H.-K. Li, M. Santosh, Z.-X. Li, H.-B. Zou, H. Wang, and H. Ye, "Precambrian evolution and cratonization of the Tarim Block, NW China: Petrology, geochemistry, Nd-isotopes and U–Pb zircon geochronology from Archaean gabbro-TTG–potassic granite suite and Paleoproterozoic metamorphic belt," J. Asian Earth Sci. **47**, 5–20 (2012).
76. C. L. Zhang, X. T. Ye, H. B. Zou, and X. Y. Chen, "Neoproterozoic sedimentary basin evolution in southwestern Tarim, NW China: New evidence from field observations, detrital zircon U–Pb ages and Hf isotope compositions," Precambrian Res. **280**, 31–45 (2016).
77. C. L. Zhang, X. T. Ye, R. E. Ernst, Y. Zhong, J. Zhang, H. K. Li, and X. P. Long, "Revisiting the Precambrian evolution of the Southwestern Tarim terrane: Implications for its role in Precambrian supercontinents," Precambrian Res. **324**, 18–31 (2019).
78. G. C. Zhao, Y. J. Wang, B. C. Huang, Y. P. Dong, S. Z. Li, G. W. Zhang, and S. Yu, "Geological reconstructions of the East Asian blocks: From the breakup of Rodinia to the assembly of Pangea," Earth Sci. Rev. **186**, 262–286 (2018).
79. B. Zheng, W. Zhu, R. Ge, H. Wu, J. He, and Y. Lu, "Proterozoic tectonic evolution of the Tarim Craton: New insights from detrital zircon U–Pb and Lu–Hf isotopes of metasediments in the Kuruktag area," Precambrian Res. **346**, p. 105788 (2020).
80. T. Zhou, R. Ge, W. Zhu, and H. Wu, "Is there a Grenvillian orogen in the southwestern Tarim Craton?" Precambrian Res. **354**, 409–424 (2021).
81. W. Zhu, B. Zheng, L. Shu, D. Ma, H. Wu, Y. Li, W. Huang, and J. Yu, "Neoproterozoic tectonic evolution of the Precambrian Aksu blueschist terrane, northwestern Tarim, China: Insights from LA-ICP-MS zircon U–Pb ages and geochemical data," Precambrian Res. **185**, 215–230 (2011).

Translated by A. Bobrov